University of Alberta

Economic Dispatch using Advanced Dynamic Thermal Rating

by

Milad Khaki

A thesis submitted to the Faculty of Graduate Studies and Research
in partial fulfillment of the requirements for the degree of

Master of Science

in

Software Engineering and Intelligent Systems

Department of Electrical and Computer Engineering

Fall 2011
Edmonton, Alberta

To my lovely wife **Nasim**

for your enduring support, patience, and true love

and

To my parents

for your love, encouragement, wisdom, and guidance

Abstract

Scientific and technology advances in electrical engineering and increasing demand for electrical energy have led to extensive research in power industry and formation of new markets for electrical energy. These developments have brought about interest and demand for power. In response to the increase in demand, the research focus is on upgrading the current infrastructure to higher capacity power transmission networks. Nevertheless, building new generating stations and transmission facilities is precluded by some environmental, social, and economic regulations. Therefore, the only feasible solution to deal with the energy requirement is to increase and optimize the capacity of existing power generation and transmission equipment.

The current thesis proposes an optimization method based on the Mixed Integer Linear Programming technique to maximize the usage of the capacity of power transmission facilities. The method employs weather-based dynamic thermal ratings, costs of power generation, and power generation constraints such as cost of start-up/shut-down and generation ramp up/down limits. The method's accuracy is increased by incorporating a spatially resolved, high-resolution thermal model of the transmission system. By utilizing this extension, the thermal limits and temperature-dependent losses of the system are identified and dynamically used in calculations.

Load forecasting is used in dispatch centers to improve generator scheduling

and minimize the costs of the entire system. The multi-snapshot characteristic of the model, which is proposed in this thesis, provides the model with the ability to consider the load and meteorological data's forecasts, further improving the model's accuracy. The performance of the model is tested by simulating a year of data from Newfoundland and Labrador Hydro power generation and transmission system, and for the weather conditions the North American Regional Reanalysis (NARR) historical dataset is used. The simulation results show that the overall costs of the system can be reduced by incorporating dynamic capacity of transmission lines and optimizing the power generation and transmission. The temperature and resistance variability of the transmission network is also analyzed and the results are provided.

Acknowledgements

I would like to express my sincere appreciation and gratitude to Dr. Petr Musilek and late Dr. Don Koval for their supervision and constant kind support during my studies and in writing this thesis. I would also like to acknowledge all members of the FACIA research group for their useful comments and support on my research. It was really a pleasure working and learning side by side them.

Milad Khaki
Edmonton, AB, Canada
July 2011

Contents

1 Introduction and Motivation 1

2 Background 4

2.1 Thermal States of Conductor 4

2.1.1 Conductor Temperature 4

2.1.2 Current Carrying Capacity 8

2.1.3 Rating Approaches 8

2.2 Economic Dispatch 9

2.2.1 What is Economic Dispatch? 10

2.2.2 Methods 10

2.3 Components of a Power Network 11

2.3.1 Generation 11

2.3.2 Transmission Lines 12

2.3.3 Loads 13

3 Thermal Model of Conductor 16

3.1 IEEE 768 Standard and Evaluating Conductor Temperature 16

3.1.1 IEEE Standard Simulations 20

3.2 Thermal States of a Conductor 30
3.3 Line Rating Methods 31
3.4 Model Evaluation 36
3.5 Thermal Rating using Numerical Weather Prediction 41
3.6 Spatial Variability Analysis 42
3.6.1 Ampacity 43
3.6.2 Temperature 45
3.6.3 Resistance Calculation 49

4 Extensions to Economic Dispatch Problem 52
4.1 Generator Cost Model 53
4.2 Power Generation Parameters 55
4.3 Voltage Drop Limitations 56
4.4 MIP Model Nomenclature 56
4.4.1 Constants and Variables of MIP model 59
4.5 MIP Model Structure 62
4.6 MIP Model Description 63
4.7 Piecewise Linear Variable Constraints 66

5 Simulation Study 68
5.1 Case study, Newfoundland and Labrador 68
5.1.1 Transmission Network 68
5.1.2 Local Weather Information 72
5.2 Static and Dynamic Thermal Rating 73
5.3 Baseload operation of hydroelectric generator 74
5.4 Comparison of different prediction frames 76

5.5 Simulation including the Voltage Drop Limit effect 85

6 Conclusions 91

6.1 Contributions 93

6.2 Future Work 94

Bibliography **95**

Bibliography 95

Appendix

List of Figures

Figure

2.1 Convection Heat loss piecewise function plots 15

3.1 Conductor temperature variations vs. Current with regard to solar absorption coefficient 17

3.2 Analysis of heat sources and sinks for a sample conductor 19

3.3 Transmission line associated heat losses/gain vs. line current 20

3.4 Transmission line associated heat losses/gain vs. line current 21

3.5 Loss-Temperature Ratio vs. wind speed 21

3.6 Loss-Temperature Ratio vs. line current 22

3.7 Losses vs. Line Temperature with regard to line current 22

3.8 The effect of angle between wind direction and conductor axis on conductor temperature 23

3.9 The effect of wind speed on conductor temperature 25

3.10 The effect of ambient temperature on conductor temperature 27

3.11 The effect of conductor elevation above sea level on conductor temperature 27

3.12 The effect of time of the day on conductor temperature 28

3.13 The effect of day of the year on conductor temperature 28
3.14 The effect of conductor axis direction from north on conductor temperature 29
3.15 The effect of conductor latitude on conductor temperature 29
3.16 Error percentages of Ampacities for different types of conductors vs. Conductor Diameter 40
3.17 Calculated Ampacities vs. published Ampacities for different types of conductors 40
3.18 Case study power transmission network schematic, including Line #32 segment details 44
3.19 Statistical parameters of ampacity each segment of line #32 44
3.20 Histogram of ampacity difference 46
3.21 Histogram indicating the frequency of each segment having maximum/minimum ampacity 46
3.22 Statistical parameters of temperature each segment of line #32 47
3.23 Histogram of temperature difference 48
3.24 Histogram indicating the frequency of each segment having maximum/minimum temperature 50
3.25 Comparison of two methods for calculating line resistance: Bottleneck and Segment by Segment methods. Bottleneck Resistance = 18.81 Ω, Separate segment resistance = 17.70 Ω 50

4.1 A Block diagram of the optimization model 62

5.1 Simplified transmission network 69
5.2 Assumed weekly load profile of St. John's 78

5.3 Statistical annual load information of St. John's 78
5.4 Assumed annual load profile of St. John's 79
5.5 Ampacity of line #31: nominal static rating (STR) and dynamic ampacity (DTR) 79
5.6 Generator scheduling results using the DTR method on a 2 week sample of load profile 80
5.7 Generator scheduling results using the STR method on a 2 week sample of load profile 80
5.8 Generator scheduling results of using hydro power plant as baseload generator 81
5.9 Total Generation Cost and Simulation Duration vs. Prediction Frame Length 89
5.10 Generator scheduling results applying 5% voltage drop constraint on a 2 week sample of load profile 89
5.11 Generator scheduling results applying 10% voltage drop constraint on a 2 week sample of load profile 90

List of Tables

Table

3.1 Line heating parameters vs. ε 19

3.2 Conductor specifications and weather parameters used for thermal model configuration 24

3.3 Rating Comparisons for different types of conductors, Part A 37

3.4 Rating Comparisons for different types of conductors, Part B 38

4.1 Comparison of the general cost values for different types of conductors 55

4.2 Constant parameters used in the MIP model 60

4.3 Variable parameters used in the MIP model 61

5.1 Generation/Demand specifications of the case study 70

5.2 Assumed generator characteristics and cost parameters in case study 71

5.3 Assumed transmission line characteristics in case study 72

5.4 Annual and seasonal comparison of simulation results using STR, DTR, and Baseload methods. 75

5.5 Results of simulation using different PFW, first part 82

5.6 Results of simulation using different PFW, second part 83

5.7 Results of simulation using different PFW, third part 84

5.8 Comparison of different PFW length 85
5.9 Simulation results using voltage drop constraints of 5% and 10% limits. 87
5.10 Simulation results of applying voltage drop constraint to the model using 5 and 10 percent limits. 88

Chapter 1

Introduction and Motivation

For the past twenty years, interest and demand for expansion of transmission capability of electric power networks have grown. The formation of electricity markets and restructuring electric power industry have increased the rate of growth as well [1]. However, this seemingly endless growth has caused a number of impediments for constructing new generating stations and transmission lines. These roadblocks include environmental, social, and economic constraints [2]. As a result, engineers, equipment manufacturers, and regulatory agencies have the problem of increasing the existing capacity of power generation facilities and transmission infrastructures.

From the generation perspective, various methods are available. These technologies have different characteristics such as capital and operational costs, performance characteristics, and environmental impacts. Therefore, the solution to power generation and transmission in every case is unique and depends on the availability of generation sources and their distance to the demand centres.

Depending on the type of power plant, there might be different capital and operation costs, performance characteristics, and environmental impact. Therefore,

optimization techniques must be applied so that the generation costs are minimized and environmental impacts are reduced. As the generation technologies depend on local resources, for example a hydro power plant requires available running water or natural water reservoir, an ideal configuration might not be available in all instances. For example, a remote hydro generating station can produce inexpensive energy and transfer it to a load centre. However, transferring the less expensive power over long distances leads to higher voltage drop and power losses.

The main objective of this thesis is to develop a mixed integer programming based optimization method to improve economic dispatch in power generation and transmission networks. In order to achieve this objective, the thesis addresses the following goals

- To use Dynamic Thermal Rating as an improved method for ampacity calculations.
- To introduce multi-snapshot simulation as a way to cope with start-up delays and costs associated with thermal power plants.
- To provide an approximation method to convert non-linear convex characteristics of power plants and transmission lines to linear piecewise equivalents that can be implemented in a linear mixed integer programming model.
- To perform segment-by-segment analysis of transmission lines to account for spatial variability of their ampacity and resistance.
- To perform simulations considering voltage drop and assess its impact on transmission of power over long distances.

- To examine the performance of the proposed model under various conditions (e.g. different seasons, varying demand, use of spinning reserve, etc.).

This thesis describes an approach to power system optimization that extends the current economic dispatch methods by considering spatially-resolved models of conductor ampacity, line resistance, and power losses. In order to incorporate different power generation technologies, this approach employs generation costs, power generation increase/decrease rates, and delays of start up/shut down. It also extends the standard optimization based on Mixed Integer Programming (MIP) by using the ampacity prediction of the power transmission line.

Chapter 2

Background

The first section of this chapter discusses the thermal states of a conductor and how conductor temperature is related to both its current and the ambient weather conditions. Ampacity or current carrying capacity is introduced in this section and different methods of calculating line rating are discussed. The next section introduces the economic dispatch and provides a brief review of several solution methods used for optimal power flow problem. The last section introduces the three main components of a power system: power sources (or power plants), transmission systems, and power sinks. The information regarding some features related to the performance, operation, and the state of subsystems are also provided.

2.1 Thermal States of Conductor

2.1.1 Conductor Temperature

While in the steady state condition, the heat transfer is balanced between the conductor and its surrounding environment [3, 4]. The conductor is assumed in a

steady state condition when load current, ambient temperature, wind velocity and solar radiation are fixed or have an approximately fixed value during a 30 minute period. The conductor heat gain is equal to the heat loss of the conductor; this relation is formulated in equation (2.1). Q_a is the heat generated by the conductor current and is calculated as $I^2 \times R$. Q_s is the heat gained through solar radiation, Q_c is heat loss due to air convection and Q_r is the heat loss of conductor with the means of radiation.

$$Q_a + Q_s = Q_c + Q_r \ . \tag{2.1}$$

In order to evaluate the generated heat by conductor, Q_a, the conductor resistance must be calculated as a function of temperature, which leads to the equation (2.2). t_c is the temperature of conductor in degrees Celsius, R_{20} is the alternative current (AC) resistance of the conductor at $20°C$, as provided in the manufacturer's datasheet (unit is $\left[\frac{\Omega}{m}\right]$). α_{20} is the temperature resistance coefficient of aluminum at $20°C$.

$$R(t_c) = R_{20} \times (1 + \alpha_{20} \times (t_c - 20)) \quad \left[\frac{\Omega}{m}\right]. \tag{2.2}$$

According to [3], heat gained from the sun can be evaluated using the following equation.

$$Q_s = \varepsilon \ S \ A \quad \left[\frac{W}{m}\right], \tag{2.3}$$

ε is solar-absorption coefficient which is approximately equal to the thermal emissivity of the conductor. S is solar radiation in $\left[\frac{W}{m^2}\right]$ and A is the projected area of the conductor in $[m^2]$. According to section 3.4.5 of the IEEE 768 standard, radiated heat loss is calculated by the following equation [5]

$$Q_r = 0.0178\ D\ \varepsilon\ \left[\left(\frac{T_c + 273}{100}\right)^4 - \left(\frac{T_a + 273}{100}\right)^4\right] \quad \left[\frac{W}{m}\right]. \tag{2.4}$$

Convection Heat Loss equations, which are more complex than the other equations, are mentioned in section 3.4 of the IEEE 768 standard [5]. Forced Convection Heat Loss, equation (2.5) is applicable at low wind speeds where the Reynolds number is ranging from 0.1 to 1,000. This range of the Reynolds number includes air velocities up to 0.61 $[\frac{m}{s}]$ for conductor diameters up to 33 mm [6].

$$Q_{c_1} = \left[1.01 + 0.372\left(\frac{D\ \rho_f\ V_w}{\mu_f}\right)^{0.52}\right]\ k_f\ K_{angle}\ (T_c - T_a) \quad \left[\frac{W}{m}\right]. \tag{2.5}$$

On the other hand, equation (2.6) can be applied at high wind speeds where the Reynolds number ranges from 1,000 to 50,000 [6]. This range includes air velocities of more than 0.61 $[\frac{m}{s}]$.

$$Q_{c_2} = \left[0.0119\ \left(\frac{D\ \rho_f\ V_w}{\mu_f}\right)^{0.6}\ k_f\ K_{angle}\ (T_c - T_a)\right] \quad \left[\frac{W}{m}\right]. \tag{2.6}$$

In summary, at any wind speed, the larger of the two convection heat loss rates values are calculated using the following equations. The convective heat loss rate is multiplied by the wind direction factor, K_{angle}, in which ϕ is the angle between the wind direction and the conductor axis

$$K_{angle} = 1.194 - cos(\phi) + 0.194\ cos(2\phi) + 0.368\ sin(2\phi). \tag{2.7}$$

Natural convection occurs with zero wind speed (still air conditions), where the rate of heat loss is shown in the following equation

$$Q_{cn} = 0.0205\ {\rho_f}^{0.5}\ D^{0.75}\ (T_c - T_a)^{1.25} \quad [W/m]. \tag{2.8}$$

The viscosity of air, air density, thermal conductivity of air, and film temperature are determined by the following equations respectively

$$\mu_f = \frac{1.458e-6\ (T_{film}+273)^{1.5}}{T_{film}+383.4} \quad [Pa-s], \tag{2.9}$$

$$\rho_f = \frac{1.293 - 1.525\times10^{-4}\ H_e + 6.379\times10^{-9}\ H_e^2}{1+0.00367\times T_{film}} \quad \left[\frac{km}{m^3}\right], \tag{2.10}$$

$$k_f = 2.424\times10^{-2} + 7.477\times10^{-5}\ T_{film} - 4.407\times10^{-9}\ T_{film}^2 \quad \left[\frac{W}{m-^\circ C}\right], \tag{2.11}$$

$$T_{film} = \frac{T_c+T_a}{2} \quad [^\circ C], \tag{2.12}$$

with the aid of these equations it is possible to maintain the balance in equation (2.1). The unknown parameter is T_{film}, because the conductor's temperature is not known. By using some non-linear numerical calculation methods, the conductor's temperature can be derived.

Figure 2.1 shows different segments of the piecewise function which is used for convection heat loss calculations. At very low wind speeds the convection heat loss is equal to natural convection heat loss in the presence of still air. For low wind speeds, resulting in low Reynolds numbers R_e, the actual convection heat loss follows equation (2.5); and for high wind speeds, which are associated with high Reynolds numbers R_e, actual convection heat loss follows equation (2.6). For simulating the plots of Figure 2.1, the following assumptions are made: the angle between the wind direction vector and conductor axis is 90 Deg, elevation above sea level is 460 m, conductor diameter is 28.12 mm, and the ambient temperature is 40 $^\circ C$.

2.1.2 Current Carrying Capacity

From the power transmission perspective, an important characteristic of a conductor is its thermal capacity, or thermal rating. The thermal rating of a conductor, also called ampacity, determines its capacity for transferring power and there are several methods for calculating it. Determination of the thermal rating of a conductor relies on solving the heat balance equation. This equation considers the heat that is gained by the conductor through internal and external heating sources and the heat which is dissipated into the surrounding environment. The important parameters that are necessary for calculating the thermal state of a conductor are its physical characteristics and surrounding ambient conditions such as temperature, normal wind component, and solar radiation [7].

2.1.3 Rating Approaches

Traditionally, the static rating is determined based on conservative weather condition assumptions to minimize the risk of exceeding the approved maximum tolerable conductor temperature. The existing approaches for calculating the static thermal rating often utilize standard unchanging weather combinations [8]. In order to calculate the static rating of a sample conductor, the equations mentioned in section 2.1 can be used. Sun heating, radiation and convection cooling, which are mentioned in equation (2.1), are assumed to be constant and their values are selected in a way to simulate the near worst case conditions. Therefore, the maximum current that can pass through the conductor can be calculated. Therefore, the methodology underutilizes the capacity. The details of evaluating the rating of conductors are discussed in Chapter 3.

The dynamic thermal rating (DTR) method is based on the observation that

the temperature, as the first limit, must be considered for the current carrying capacity of a circuit. This parameter is affected by the ability of the component to dissipate heat to the environment which is the result of the resistance heating. Heat dissipation depends on external conditions such as ambient temperature, or wind speed [9]. On the other hand, dynamic thermal ratings are, rather than worst-case, generally based on actual weather and pre-load conditions. Therefore, it is expected that they add some extra capacity in comparison with static ratings. However, real-time field monitoring and continuous re-calculation of heat balance equations are required to the calculate conductor temperature to prevent overheating of the equipment [10].

2.2 Economic Dispatch

To avoid unnecessary emissions, environmental concerns have introduced new constraints and the electric power system dispatches are scheduled to minimize the total fuel cost. A review of algorithms for environmental-economic dispatch is provided in [11]. Therefore, in the current deregulated power industry, the concept of *Economic Dispatch (ED)* has become an essential part of the operation and planning of electric power systems. The basic idea of ED involves scheduling the active generation units in a way that while the sum of all costs is minimized, the demand and all operational constraints are satisfied [12]. In other words, the output of each individual unit is controlled so that the generation expenses of the entire system are minimized [13].

2.2.1 What is Economic Dispatch?

Economic dispatch is defined as the process of allocating generation values to the generating resources, so that the system demand can be supplied entirely and most economically [14]. The efficiency of the ED algorithm is directly affected by the accuracy of the generation costs calculation. Several methods have been proposed and incorporated to solve ED problems. These methods range from linear programming [15] through inverse incremental cost functions [16] to heuristic approaches, such as particle swarm optimization [12]. The review of the various economic dispatch methods is provided in the next subsection.

2.2.2 Methods

Linear Programming is a common and effective method to solve the ED problem. As a requirement, in linear programming formulation, objective function and constraints must be linearized and only positive variables are accepted. The Mixed Integer Programming method used in the current thesis is an extension of the linear programming method. It is discussed in detail in Chapter 4. Another example of this method is provided by Chung et al. [17]. The presented method in [17] uses a recursive linear programming based approach to minimize line losses and to locate the optimal capacitor location in a distribution system. Cost-benefit is calculated for a 14-bus case study. In order to apply ED to large-scale linear programming problems, Interior Point (IP) is an efficient method which is proposed in [18]. The IP method focuses on finding improved search directions strictly in the interior of a feasible solution space.

The next method used for ED is Quadratic Programming (QP). QP can be defined as a special case of nonlinear programming with quadratic objective function

and linear constraints. Momoh et al. have presented a generalized quadratic-based model for economic dispatch problems [19]. Nonlinear programming (NLP) is the solution for nonlinear objective function and constraints. Zhu et al. proposed a nonlinear convex network flow programming (NLCNFP) model and algorithm for solving the security-constrained multi-area economic dispatch (MAED) problem [20]. The model is solved by using a combination of quadratic programming and network flow programming. This feasible and effective method is applied to a power network with four interconnected nodes, and the results are provided.

There are several other methods which can be applied to ED problems such as Artificial Neural Networks [21], Genetic Algorithms [22], Evolutionary Programming [23], Particle Swarm Optimization [24], and Ant Colony Optimization [25].

2.3 Components of a Power Network

Electric power systems are comprised of three main components: power sources (or power plants), energy delivery systems, and power sinks, usually called load centres. Optimization of these power systems under a stochastic electricity demand requires prior knowledge regarding certain features related to their performance, operation, and the state of their subsystem. The following subsection provides basic background information about these components.

2.3.1 Generation

Electricity generation is defined as converting other sources of energy, such as solar, nuclear, kinetic, and chemical, to electrical. Electrical power is mostly generated in power stations by electromechanical generators. These generators are

usually driven by the kinetic energy of the running water or thermal energy. The heat engines are generally fuelled by thermal energy generated by chemical combustions of fossil fuel or nuclear fusion.

As thermal power plants use fossil fuel to generate electrical energy, the power produced by them is relatively more expensive than the power generated by hydro generators. In addition, scientists and environmentalists agree that the emission of the pollutant gasses and carbon dioxide by fuel driven power plants account for a significant share of the world's greenhouse emissions. Therefore, the ideal generation scenario for a multi-source power network is to increase the generation share of hydro plants and reduce emissions. The approach used in this thesis simulates power plants as sources of power in a transmission network model using mathematical rules in an attempt to minimize the cost of generated power.

2.3.2 Transmission Lines

Transmission lines are considered the infrastructure of power transmission industry. The most common means of power transfer are overhead lines and underground cables. Generally, electrical energy is transmitted in the alternating current form, which is the simplest form of transferring the bulk of power over long distances. In order to reduce the resistive losses of the transmission line, after producing power at a generating station, the voltage is raised to a higher level, such as 63 kV, 230 kV, and 500 kV, and the voltage is lowered back to consumer level at distribution centres, such as 110V or 220V. In comparison with high voltage AC (HVAC), high voltage direct current (HVDC) transmission lines are more efficient and impose less loss to the transmission system. For example, the additional power for energizing an HVAC transmission line is not required in HVDC lines and the transmission line is

more immune to the effects of its reactive components. However, because the conversion equipment of this form of transmission is more expensive, currently HVDC transmission is only used for long distance transmission.

In this thesis, a sample transmission network in Newfoundland and Labrador is studied and an optimization method is proposed to reduce the transmission losses in the entire network. Electrical energy is transferred using HVAC technology and the transmission network is described in more details in Chapter 5. The goal mentioned in subsection 2.3.1, reducing greenhouse gas emissions and decreasing generation costs, is achieved by utilizing dynamic thermal rating to increase the ampacity of transmission lines. By increasing the capacity of the transmission network, it would be possible to draw more power from distant hydro generators, which are less pollutant and expensive, and transfer it to the demand centres. The results of this study are provided in detail in chapter 5.

2.3.3 Loads

Electrical energy generation is always accompanied by its consumption. This is due to the fact that so far it has not been possible to store this type of energy in bulk form. Therefore, it is necessary to generate the energy only when there is a demand for it. Load management, a critical task in power network operation centres, is responsible for keeping the balance between generation and demand. It involves analyzing historical demand profiles and using them to produce short-term forecasts. Changing the generation amount of a power plant requires a certain amount of time, depending on the type of generator from a couple of hours up to a few days. Therefore, the short term forecasts are quite important. If the increased rate of demand goes beyond the generation rate, the network operators are forced to find additional

supplies of energy or find ways to reduce the load immediately. If the balance is not restored in the required time frame, it could be followed by catastrophic failures of the power systems such as blackouts, destruction of generation and transmission equipment.

In order to simulate the demand prediction, the load profile used in this study is generated as a combination of the typical load profile of a city referred to by Espinoza et al. and the statistical load data of the St. John's city, Newfoundland [26]. The simulations in this study are designed in a way to nearly saturate the network's generation and transmission capacity, with the purpose of analyzing the performance of the optimization method under such critical conditions.

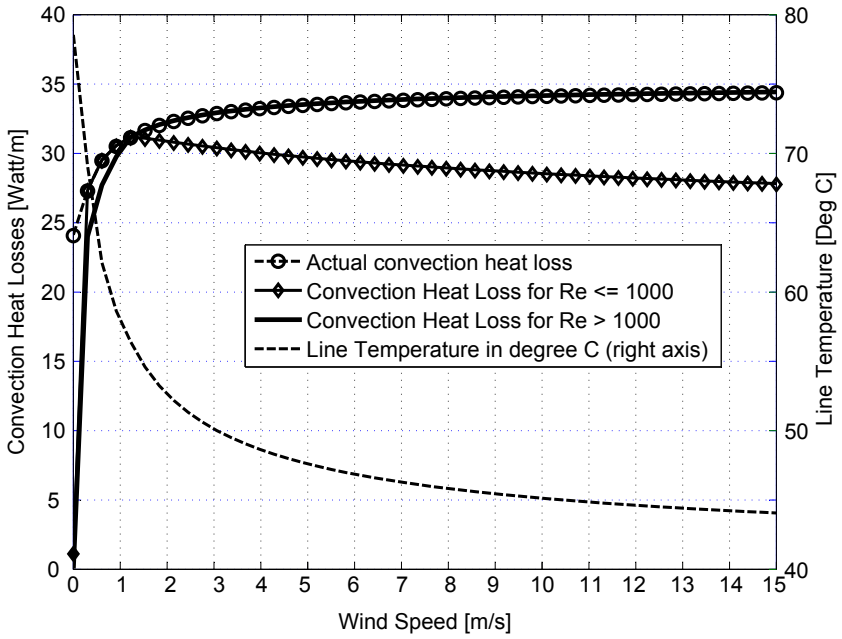

Figure 2.1: Convection Heat loss piecewise function plots (Left Axis) and Conductor Temperature (Right Axis) vs. Wind Speed.

Chapter 3

Thermal Model of Conductor

3.1 IEEE 768 Standard and Evaluating Conductor Temperature

In order to derive the temperature, various solving methods based on iteration can be used. The Newton-Raphson method is used to solve the equation in this research. To conform to this method, equation (2.1) should be rearranged as follows

$$Q_a + Q_s - Q_c - Q_r = 0 \quad \Rightarrow \quad F(T_c) = Q_a + Q_s - Q_c - Q_r = 0, \tag{3.1}$$

T_c is then evaluated using the following equation. In each iteration the calculated answer will be in closer proximity to the exact answer. Derivation of the function can be accomplished using sym (symbol) and $diff$ methods in matlab.

$$T_{c_{(new)}} = T_{c_{(old)}} - \frac{F(T_{c_{(old)}})}{\acute{F}(T_{c_{(old)}})} \tag{3.2}$$

Figure 3.1 demonstrates variations of temperature versus line current with regards to changing the solar absorption coefficient from 0.0 to 1.0. As the line current increases, the resistive losses of the line would increase as well. As a result, the temperature of the conductor would rise and cause more dissipation of power through radiation and convection. The following assumptions are made for the simulation of this figure: the wind speed has the constant value of 0.61 $\frac{m}{s}$ which is the equal amount for natural convection, the ambient air temperature is 20 $[^{\circ}C]$, the angle between wind direction and conductor axis is 90 Deg, the conductor diameter is 44.76 mm, and the elevation above sea level is 1024 m.

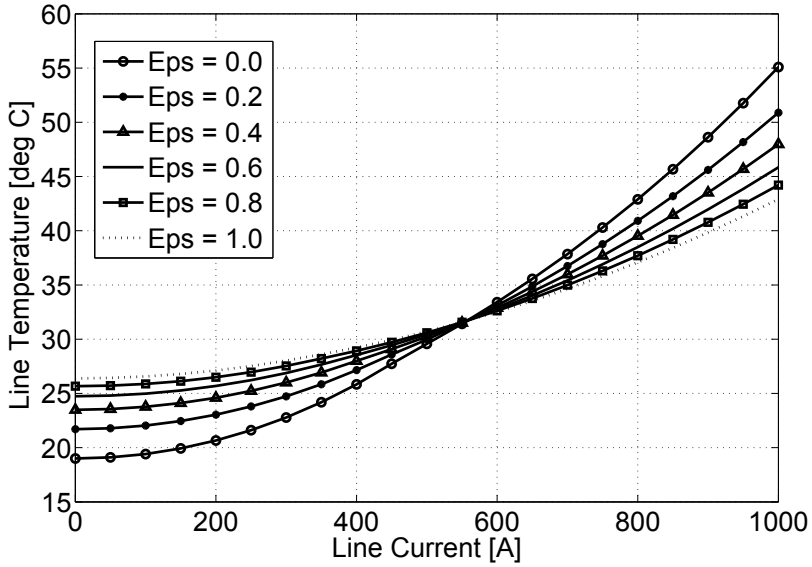

Figure 3.1: Conductor temperature variations $[^{\circ}C]$ vs. Current [A] with regard to Solar Absorption Coefficient ε.

It is demonstrated in the above graph that when the line current is zero, the temperature of the line is more than the ambient temperature. This is due to the fact that the line would still gain heat from the solar radiation and its temperature

would increase above the ambient temperature. When ε is zero, meaning that the line does not gain any heat from solar radiation, the conductor's temperature will be quite close to its ambient (which is $20°C$). In addition, for high currents passing through the power line, the temperature of a line with smaller ε is higher. As the line with lower ε can radiate less energy, its temperature will remain higher than a similar line with more heat radiation capacity.

Table 3.1 shows the different elements of the heat balance equation when the solar absorption value of the conductor, ε, changes from 0 to 1. Figure 3.2 shows the variations of the amount of heat sources and sinks of a sample conductor with regards to changes of wind speed. The wind speed ranges from 0 to 10 $[\frac{m}{s}]$. In these plots, current is assumed to be the constant value of 460 A. In the case of still air, which means that the wind speed is approximately zero (minimum natural convection heat loss), as the wind speed increases, the convection heat loss increases as well and eventually would saturate at about 2 $[\frac{m}{s}]$. When convection heat loss is minimal, radiation is the only way of releasing thermal energy; hence, it has its maximum amount at the beginning. By increasing the wind speed, radiation loss effect reduces gradually and as the conductor temperature reaches the ambient temperature it eventually descends to zero.

The heat that is gained from solar radiation, which is a function of the conductor's physical characteristics, is constant regardless of the wind speed and conductor temperature. Resistive loss mostly depends on the resistance and current of the conductor. However, as shown in equation (2.2), the resistance is also a function of its temperature. Therefore, at low wind speeds when the temperature of the conductor increases, the resistive loss increases as well.

Figures 3.3 and 3.4 show the variations of different loss components with regards

Table 3.1: Line heating parameters vs. ε at the constant current of 1000 $[A]$

Units	ε	Conductor Temperature $[\frac{Watt}{m}]$	Joules Losses ^oC	Sun Warming $[\frac{Watt}{m}]$	Convection Cooling $[\frac{Watt}{m}]$	Radiation Cooling $[\frac{Watt}{m}]$
	0.0	55.1	31.49	0.0	31.49	0.0
	0.2	50.9	30.87	2.16	27.06	5.96
	0.4	48.0	30.44	4.31	24.07	10.68
	0.6	45.8	30.12	6.47	21.91	14.67
	0.8	44.2	29.87	8.62	20.28	18.22
	1.0	42.9	29.68	10.78	19.00	21.46

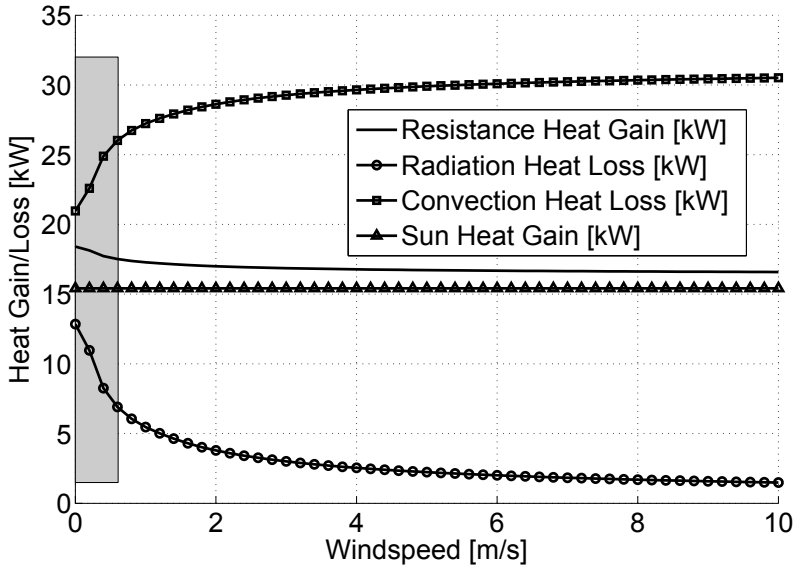

Figure 3.2: Analysis of heat sources and sinks for a sample conductor with the constant current of 460 [A].

to changes of line current. Wind speed is assumed to have the constant value of 0.61 $[\frac{m}{s}]$. Apart from sun heat gain that remains constant the other three variables will exponentially grow with the rise of line current.

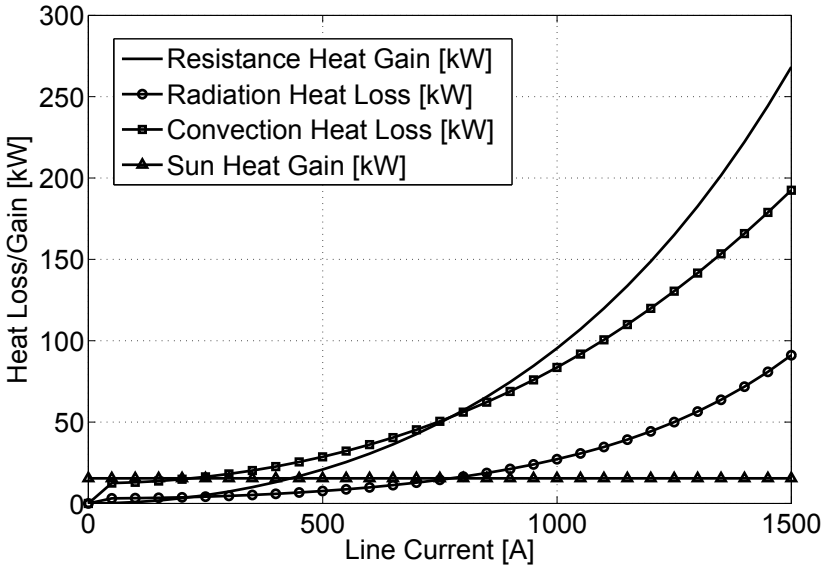

Figure 3.3: Transmission line associated heat losses/gain $[\frac{W}{km}]$ vs. cine current $[A]$. Assumptions: wind speed = 0.61 $[\frac{m}{s}]$, conductor type = Drake, ambient temperature = $40°C$, solar absorption coefficient (ε) = 0.5, current range = [0 1500] $[A]$

Figure 3.5 shows the ratio of loss and temperature versus wind speed. The line current is assumed to have the constant value of 460 A. Figure 3.6 shows the ratio of loss and temperature versus line current. Wind speed is assumed to have the constant value of 0.61 $[\frac{m}{s}]$. Figure 3.7 shows variations of line losses versus conductor's temperature, when line current varies from 200 A to 1000 A.

3.1.1 IEEE Standard Simulations

This subsection illustrates and analyzes the simulation results of the effect of various weather parameters on the line temperature. In order to simulate the line

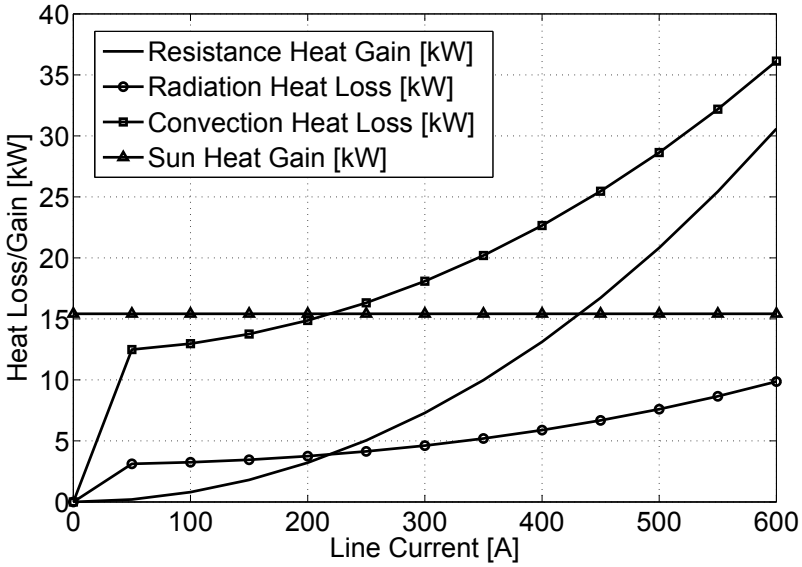

Figure 3.4: Transmission line associated heat losses/gain $[\frac{W}{km}]$ vs. line current $[A]$. assumptions: wind speed = 0.61 $[\frac{m}{s}]$, conductor type = Drake, ambient temperature = $40°C$, solar absorption coefficient (ε) = 0.5, current range = [0 600] $[A]$

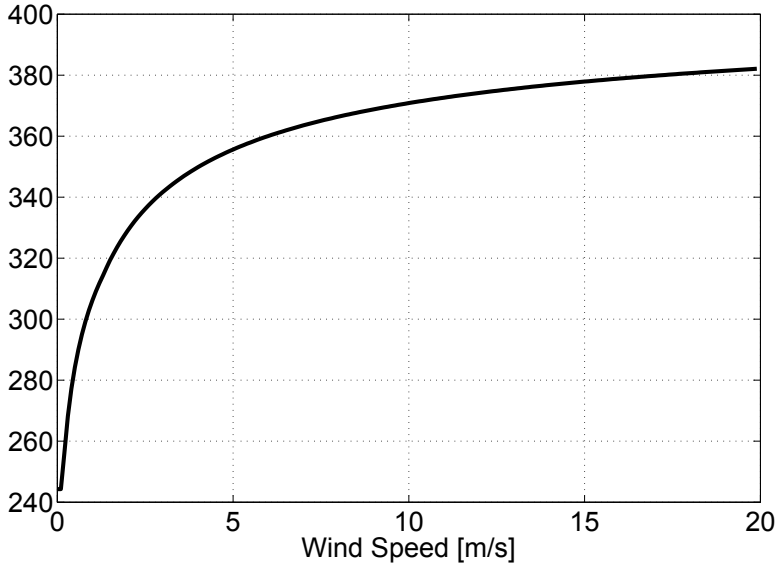

Figure 3.5: Loss-Temperature Ratio vs. wind speed $[\frac{m}{s}]$. assumptions: conductor type = Drake, ambient temperature = $40°C$, solar absorption coefficient (ε) = 0.5, line current = 460 $[A]$

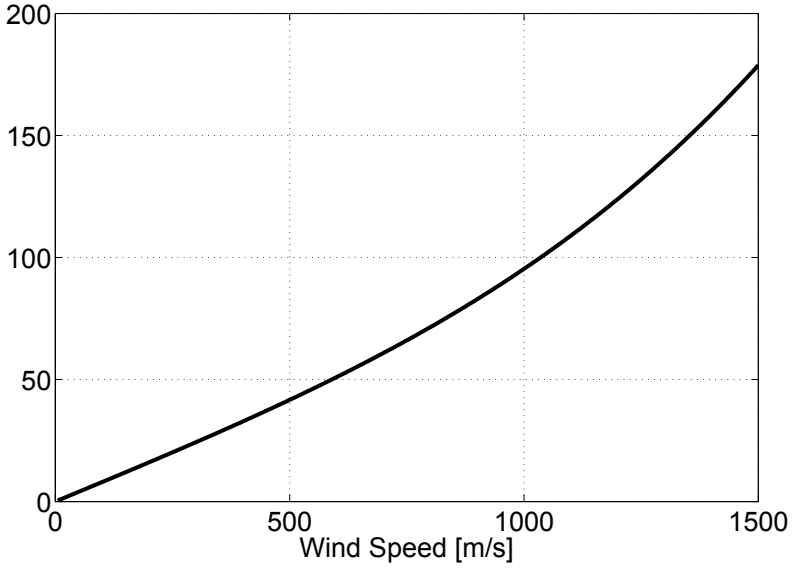

Figure 3.6: Loss-Temperature Ratio vs. line current [A], wind speed is 0.61 $[\frac{m}{s}]$

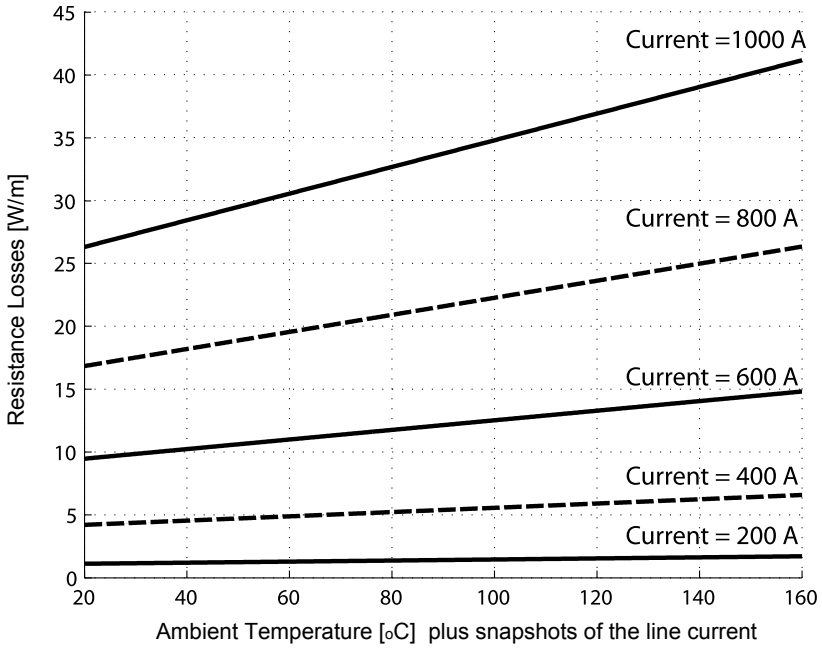

Figure 3.7: Losses $[\frac{W}{m}]$ vs. line temperature $[^{\circ}C]$ with regard to line current

model, the equations discussed in the beginning of the chapter and section 3.1 are utilized. Table 3.2 shows the default values that are used for the line model.

In each figure, all conductor parameters are kept constant except the variable which is being analyzed. In this manner the effect of each variable on the conductor's temperature is illustrated exclusively. Figure 3.8 shows the effect of changing angle between the conductor axis and wind direction axis. If the wind blows in parallel with the conductor axis, the effect of cooling is negligible. However, as the angle increases cooling is more pronounced and when the two mentioned axes are perpendicular it reaches the maximum and the temperature is minimized.

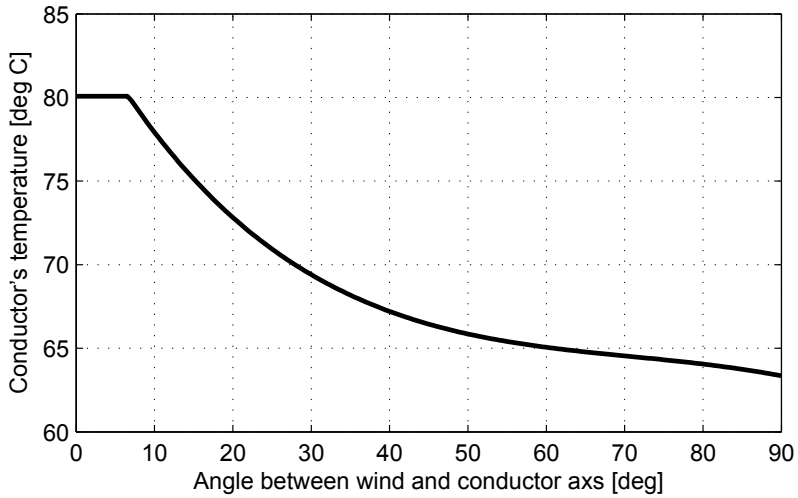

Figure 3.8: The effect of angle between wind direction and conductor axis on conductor temperature, based on the parameters from Table 3.2

The effect of wind speed as the next parameter is illustrated in Figure 3.9. By increasing the wind speed, the effect of convective cooling would be increased as well. The figure also confirms this phenomenon, indicating that for wind speed values of more than 5 $[\frac{m}{s}]$ the cooling effect would saturate and does not change the conductor's temperature significantly.

Table 3.2: Conductor specifications and weather parameters used for thermal model configuration

Parameter	Default Value	Unit	Symbol
Current	520	$[A]$	I
Ambient Temperature	40	$[^oC]$	T_a
Wind speed	0.61	$[\frac{m}{sec}]$	V_w
Diameter	28.12	$[mm]$	D
Resistance at 25 $[^oC]$	0.07284	$[\frac{\Omega}{km}]$	
Conductor resistance at 75 $[^oC]$	0.08689	$[\frac{\Omega}{km}]$	
coefficient of Emissivity,	0.5		ε
coefficient of Absorption,	0.5		ε
Elevation above sea level	460	m	H_e
Orientation	0	Deg	ϕ
Latitude	30	Deg	Lat
Time of Day	11		
Day of Year	161		
Air Type (Industrial/Clear)	clear		

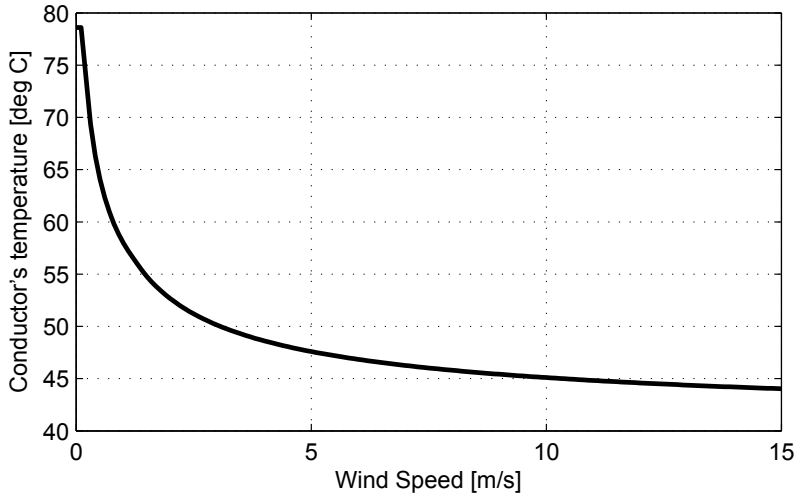

Figure 3.9: The effect of wind speed on conductor temperature, based on the parameters from Table 3.2

Figure 3.10 shows the effect of changing ambient temperature on conductor temperature. The relation is a simple linear offset. Increasing the ambient temperature results in an equivalent increase in the conductor's temperature. Figure 3.10 shows how changing the elevation of a conductor affects its temperature. According to the figure, by increasing the conductor's elevation, the conductor's temperature will increase in a linear fashion. Figure 3.12 describes the effects of time of day on the conductor's resistance. The effect is negligible during the hours before sunrise and after sunset; it will rise to the maximum during noon and will reduce back to zero during the afternoon and evening hours. It should also be noted that the heat gain from the sun is also a function of the day of the year and the conductor's coefficient of emissivity, ε.

Figure 3.13 illustrates the effects of the day of the year on the conductor's temperature. This effect is the result of the sun's angle of radiation towards the earth and the conductor. This effect is quite small and changes the temperature about $4°C$. Figure 3.14 shows the effect of conductor axis direction from north on its temperature. The simulation results are calculated assuming that the angle between wind and conductor axis remains constant. The observed changes are the results of variations of solar radiation on the conductor's surface which is quite small compared to the other parameters. Figure 3.15 provides the results of changing the conductor's latitude on its temperature. Changing the latitude will only change the sun's angle of radiation which in turn changes the temperature and has a very small share in calculating the conductor's temperature.

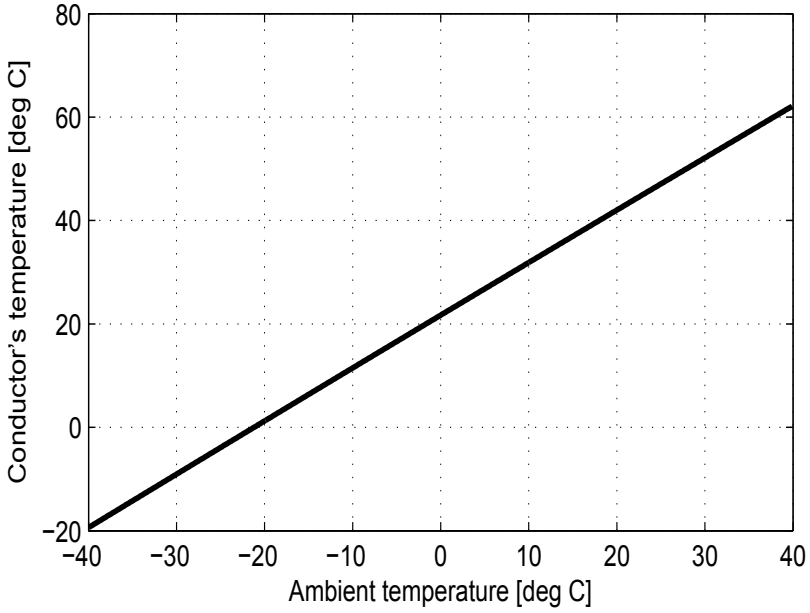

Figure 3.10: The effect of ambient temperature on conductor temperature, based on the parameters from Table 3.2

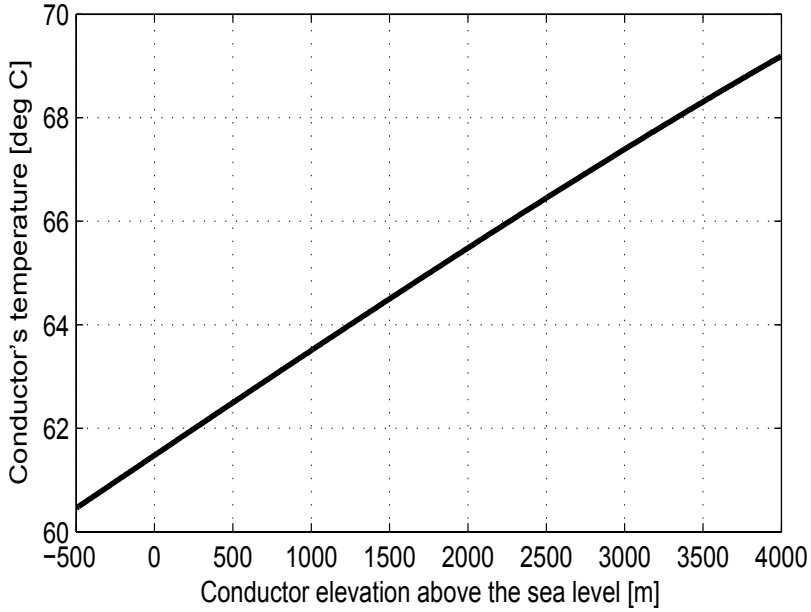

Figure 3.11: The effect of conductor elevation above sea level on conductor temperature, based on the parameters from Table 3.2

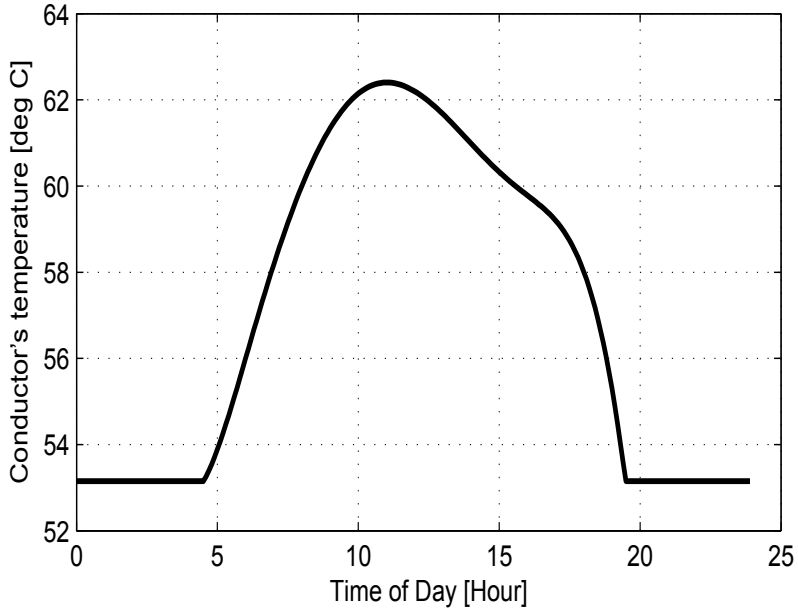

Figure 3.12: The effect of time of the day and sun heat gain on conductor temperature based on the parameters from Table 3.2

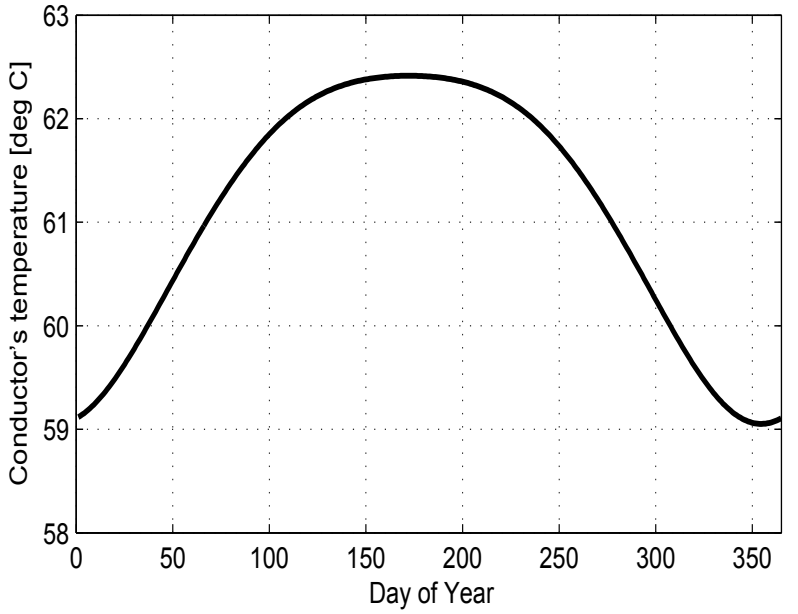

Figure 3.13: The effect of day of the year (sun heat gain) on conductor temperature, based on the parameters from Table 3.2

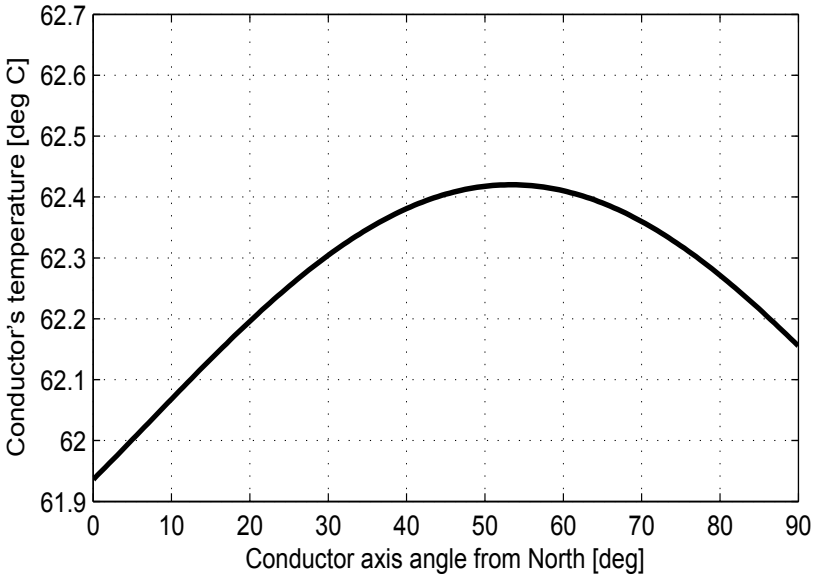

Figure 3.14: The effect of conductor axis direction from north on conductor temperature, based on the parameters from Table 3.2

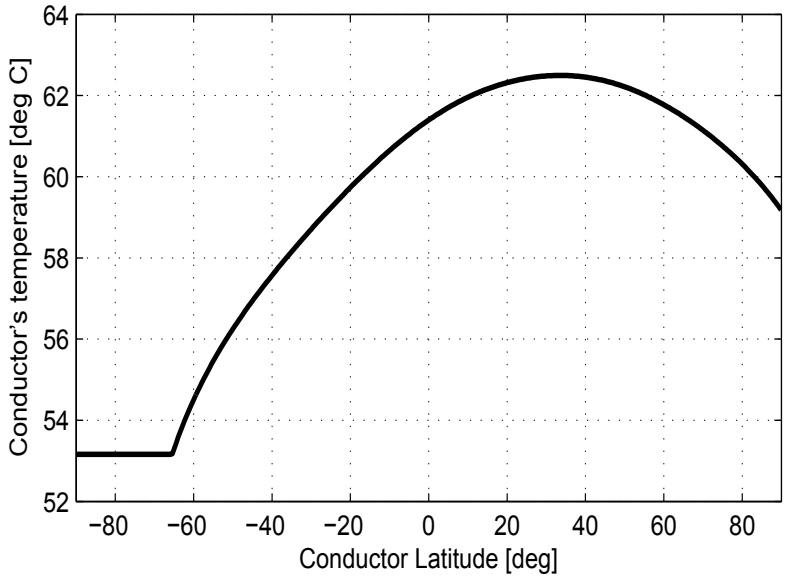

Figure 3.15: The effect of conductor latitude on conductor temperature, based on the parameters from Table 3.2

As previously noted, the IEEE Standard 738-2006 describes the thermal model of a transmission line with a number of simplifications. In this standard, Precipitation Cooling is one of the parameters that have been excluded from the thermal model of the transmission line. Pytlak et al. propose an extended thermal model of the transmission line that focuses on modeling the heat loss due to rain or snow falling on the conductor surface [7]. By using the mentioned model an additional capacity for the transmission line can be achieved. However, during the research for this thesis, the new thermal model was under development and could not be used for the calculations. Therefore, the thermal rating model of the transmission line, used in the Dynamic Thermal Rating Algorithms, is the method that the IEEE 768-2006 standard provides [5].

3.2 Thermal States of a Conductor

Another important aspect of a transmission line model which is necessary for controlling a conductor's temperature is its working state. Different operating states of conductor are

- Steady State
- Dynamic State
- Transient State

During normal operating conditions, when there is a balance between the heat that is gained and lost, the conductor is in a steady state condition. In this state the transmission line's current and weather conditions are assumed to be constant and stable; the temperature of the conductor is assumed to be uniform along each segment.

The dynamic condition is defined as a sudden change in current. There are a variety of sources for this rapid change; one example is the transfer of power from one line to another because of a fault. The switching causes a dynamic condition in the latter line. Since the line's temperature will rise with a relatively large time constant, during a short-time dynamic condition the temperature roughly remains constant and the line would be able to bear a short overload current without reaching the overheating limit.

On the other hand, transient conditions arise in the event of a short-circuit or lightning current. During a transient condition, there is no heat exchange with the environment; therefore, adiabatic conditions can be assumed [4].

3.3 Line Rating Methods

The rating of a transmission line or its *ampacity* is defined as the maximum allowed current to keep the temperature of a transmission conductor within an acceptable range. There are several factors that limit the amount of power that can pass through a power transmission line. They include voltage drop, phase shift and voltage unstability, and thermal limit [10]. The chief constraint that limits the transfer of power is the thermal limit. Based on this method the limiting amount of current is defined as the current that causes the conductor to reach its critical temperature. At the critical temperature of a conductor the aging rate will increase exponentially. Some of the examples of line aging are as follows [10]

- Annealing of aluminum or copper strands
- Loss of paper tensile strength or formation of gas bubbles in underground cables

The increase of temperature will also cause premature damages to the other power transfer equipment and devices as well; for instance, the silver plating of contacts and circuit breakers might get damaged as a result of over-temperature operation. Increased temperature will also cause line sag in the case transmission lines. The length increase of a transmission line caused by heating is called *line sag*. Line sag is expected and tolerated to some extent in all power transmission systems. However, when the length of a line increases a certain threshold, the line starts to anneal and its physical characteristics will change permanently. Another reason to avoid excessive sag is that it violates the standard safety distance from the ground. The line might also get entangled with the trees and terrain below and may cause a fire and/or power failure.

In order to avoid these problems or minimize their impact, thermal limitation based line rating is employed. Based on the utilization of states of the conductor and weather conditions, transmission line rating methods are classified as several methods such as static and dynamic. In the following subsections these two methods of calculating the ampacity of a power transmission line are described.

Traditionally, to avoid exceeding the maximum allowable conductor temperature, static thermal rating, the most common rating approach, was used. Due to operating practices driven by safety and reliability requirements [27], the assumptions used to derive STR are very conservative. These assumptions in some cases involved the worst case scenario for a transmission line such as highest ambient air temperature, high solar radiation, and low wind speed [28].

The existing methods for determining static conductor thermal ratings often utilize standard fixed weather conditions. Such procedures are conservative and are only used for their simplicity and reliability. Another reason for widespread use of

the static line rating is that there is no need for constant monitoring of the power line's parameters. As expressed, the static line rating is not a flexible and adaptive method; the maximum flexibility that is expected from static line rating is that of utilizing seasonal ratings for winter and summer. However, during the season the line rating remains constant. In addition, the transmission systems that use STR are greatly underutilized.

Obviously, since this method is based on near worst case scenario, it results in under-utilization of conductor capacity. Some examples of worst case scenarios that are mentioned in [29] are as follows

- For overhead lines, low wind speed (e.g., 0.61 $[\frac{m}{s}]$) and high ambient temperature (e.g., 40 $[^{\circ}C]$)
- For power transformers, a high 24 hour average ambient temperature (e.g., 40 $[^{\circ}C]$).
- For underground cables, low soil thermal resistivity (e.g., 90$[\frac{^{\circ}C \times cm}{W}]$)

In today's competitive energy market, there is a need to maximize the capacity of transmission lines. In other words, it is desirable to avoid losing the capacity of the line by using static line rating. As mentioned in section 3.3, rating of transmission lines is calculated based on the thermal limit of the conductor. As the state of transmission line and weather parameters affects the line's temperature, the thermal rating is not constant.

Douglass et al. indicate that the most limiting devices in a power transmission system are conductors, current transformers, and power transformers [29]. Hence, in order to expand the capacity of a network, the capacity of transmission lines that are considered as the bottlenecks should be increased. For this purpose, dynamic thermal

rating systems can be employed in transmission systems to overcome the problems of STR. DTR systems are viewed as effective tools to expand the throughput of transmission systems without the high environmental and financial costs which are associated with building new lines [30].

DTR systems, since their introduction in 1977, have been the subject of many research studies [31]. Ciniglio et al. used DTR together with favourable weather conditions to increase the ampacity of the Idaho regional transmission system [32]. The effects of using DTR on different parts of transmission systems are examined in [10]. Applications of conventional DTR to the problems of electrothermal coordination, augmenting power transfer capability, and network congestion management are presented in [30] and [33]. The range of studies utilizing DTR methods vary from determination of current line capacity, through assessment of line thermal aging, to comparison of STR and DTR performances [4, 34].

Dynamic Thermal Rating (DTR) systems incorporate various means to calculate ampacity ratings such as sensor networks, statistical models and/or current weather conditions. DTR systems offer the power transmission system operators with real-time ampacity ratings. Compared to STR, the DTR method mostly increases the line's ampacity. This is due to the fact that STR methods are based on conservative assumptions of the state of the transmission line. Constant monitoring of a set of atmospheric and line operating conditions, enables additional power to be transferred through the power transmission network without installing new transmission towers and lines or upgrading the current infrastructure [7].

The efficiency gain of a power transmission system, using the DTR method, to a great extent depends on the characteristics and specific parameters of each network. Therefore, the reports show different ampacity gain in each case. While Douglass et

al. reported a 5% to 15% efficiency gain using the DTR method [29], there is a report of ampacity and power gain of 5% up to 20% in [10].

Dale et al. have described the following methods for dynamic thermal rating [4].

- Weather-Dependant System
- Temperature Monitoring System
- Tension monitoring system
- Sag monitoring
- Distributed fibreoptic sensors
- Probabilistic Rating Methods

Based on the style of measuring the transmission line data, the DTR systems are categorized into two subgroups: direct and indirect line rating systems [4]. In a direct system, the sensors and monitors are in direct contact with the transmission lines or the towers in between. Some examples are on-cable temperature sensors, donut sensors and tension monitors. In such cases, installing or maintenance will force the whole system or some parts of it to be shut down and taken out of service. On the contrary, in indirect systems, only weather conditions are monitored along the transmission line route and the actual parameters of the conductor, such as temperature, are not directly monitored. It is possible to monitor the sag using a laser beam at the middle of the conductor between anchor towers. The ampacity of the line is then calculated based on the line sag and weather data.

3.4 Model Evaluation

In order to verify the accuracy of the line ampacity calculation, the results were compared with the published data by ABB© [35], Phoenix Wire© [36], and SURAL© [37]. Tables 3.3 and 3.4 show the results of calculated static ampacity for different kinds of conductors along the values from the datasheets published by the mentioned manufacturers.

Table 3.3: Rating Comparisons for different types of conductors, Part A. based on the results published by 3 manufacturers: ABB©, Phoenix Wire©, and Sural©

Conductor Name	Circular Mils	Strands AL/St	Outside Diameter	Weight ABB lb/1000ft	Weight SURAL lb/1000ft	Weight Phoenix Wire lb/1000ft	ABB Ampacity	SURAL Ampacity	P.W. Ampacity	Calculated Ampacity
Falcon	1,590,000	54/19	1.545	2,041.1	2,044.0	2,042.0	1,380	1,359	1,370	1383
Parrot	1,510,500	54/19	1.506	1,938.8	1,940.0	–	1,340	1,318	–	1340
Plover	1,431,000	54/19	1.465	1,836.9	1,840.0	–	1,300	1,275	–	1293
Martin	1,351,000	54/19	1.424	1,734.8	1,737.0	1,735.0	1,250	1,232	1,240	1249
Pheasant	1,272,000	54/19	1.382	1,632.8	1,635.0	1,634.0	1,200	1,187	1,195	1202
Grackle	1,192,500	54/19	1.338	1,530.7	1,533.0	1,531.0	1,160	1,140	1,150	1156
Finch	1,113,000	54/19	1.293	1,428.8	1,432.0	1,430.0	1,110	1,093	1,100	1106
Curlew	1,033,500	54/7	1.246	1,329.4	1,330.0	1,329.0	1,060	1,047	1,055	1057
Cardinal	954,000	54/7	1.196	1,227.1	1,228.0	–	1,010	996	–	1005
Canary	900,000	54/7	1.162	1,157.6	1,159.0	–	970	961	–	968
N/A	874,500	54/7	1.146	1,125.0	–	–	950	–	–	951
Condor	795,000	54/7	1.093	1,022.5	1,023.0	1,022.0	900	889	895	895
Drake	795,000	26/7	1.108	1,092.8	1,094.0	1,093.0	900	907	905	908
Mallard	795,000	30/19	1.14	1,234.3	1,235.0	1,234.0	910	918	915	915
Stilt	715,500	24/7	1.036	920.3	921.8	–	830	844	–	838
Starling	715,500	26/7	1.051	983.5	984.7	984.0	840	849	850	846
Redwing	715,500	30/19	1.081	1,110.8	1,110.0	1,109.0	840	859	860	853
Flamingo	666,600	24/7	1	857.4	858.8	858.0	800	807	810	794
Rook	636,000	24/7	0.977	818.0	819.1	818.0	770	784	785	775
Grosbeak	636,000	26/7	0.99	874.2	875.1	874.0	780	789	790	786
Egret	636,000	30/19	1.019	987.3	988.0	987.0	780	798	795	792
Peacock	605,000	24/7	0.953	778.2	779.6	779.0	750	760	760	754
Squab	605,000	26/7	0.966	831.6	832.2	831.0	760	765	765	753
Dove	556,500	26/7	0.927	765.0	766.0	765.0	730	726	725	719

Table 3.4: Rating Comparisons for different types of conductors, Part B. based on the results published by 3 manufacturers: ABB©, Phoenix Wire©, and Sural©

Conductor Name	Circular Mils	Strands AL/St	Outside Diameter	Weight ABB lb/1000ft	Weight SURAL lb/1000ft	Weight Phoenix Wire lb/1000ft	ABB Ampacity	SURAL Ampacity	P.W. Ampacity	Calculated Ampacity
Eagle	556,500	30/7	0.953	868.9	871.8	871.0	730	734	735	725
N/A	500,000	30/7	0.904	780.7	–	–	690	–	–	680
Hawk	477,000	26/7	0.858	655.7	656.0	655.0	670	659	660	655
Hen	477,000	30/7	0.883	744.9	747.3	746.0	670	666	665	660
Ibis	397,500	26/7	0.783	546.4	546.6	546.0	590	587	585	584
Lark	397,500	30/7	0.806	620.6	622.6	622.0	600	594	595	588
Linnet	336,400	26/7	0.721	462.5	462.5	462.0	530	529	530	526
Oriole	336,400	30/7	0.741	525.4	527.1	526.0	530	535	535	530
Ostrich	300,000	26/7	0.68	412.5	412.7	412.0	490	492	490	490
N/A	300,000	30/7	0.7	468.4	–	–	500	–	–	494
Partridge	266,800	26/7	0.642	366.7	367.2	366.0	460	475	455	455
N/A	266,800	6/1.	0.633	341.3	–	–	460	–	–	412
Penguin	4/0.	6/1.	0.563	292.0	291.1	291.0	340	357	360	372
Pigeon	3/0.	6/1.	0.502	231.6	230.7	230.0	300	315	315	324
Quail	2/0.	6/1.	0.447	183.7	183.0	183.0	270	276	275	281
Raven	1/0.	6/1.	0.398	145.6	145.3	145.0	230	242	240	244
Robin	1	6/1.	0.355	115.5	115.1	115.0	200	212	210	212
Sparrow	2	6/1.	0.316	91.7	91.3	91.2	180	184	185	184
Sparate	2	7/1.	0.325	107.2	106.7	107.0	180	184	185	186
N/A	3	6/1.	0.281	72.7	–	–	160	–	–	161
Swan	4	6/1.	0.25	57.6	57.4	57.4	140	140	140	139
Swanate	4	7/1.	0.257	67.4	67.0	67.0	140	140	140	140
N/A	5	6/1.	0.223	45.6	–	–	120	–	–	121
Turkey	6	6/1.	0.198	36.2	36.1	36.0	100	105	105	105

Figure 3.16 shows the results of STR calculations using the proposed method based on the IEEE 738-2006 standard. The error percentage is calculated based on the following equation

$$Error = \frac{PublishedAmpacity - CalculatedAmpacity}{PublishedAmpacity} \times 100\% \tag{3.3}$$

According to the figure, the conductors' errors are arranged by their diameter on the x axis. It shows that there is a considerable difference in calculating static ampacity between different manufacturers for small conductor diameters. However, as the diameter increases, this error starts to decrease. However, the difference does not indicate that there is an actual error in calculation of ampacity. It could be related to the fact that each manufacturer has a threshold for its conductor's ampacity and this threshold might not be equal. This threshold would only affect the conductors with lower diameter and would be negligible in larger high capacity ones.

Figure 3.17 shows the ampacities calculated using the proposed method versus the ampacities published by the ABB Company [35]. Every point on the straight line indicates that the calculated result and the provided ampacity are the same for that conductor specification. However, if the point is not located on the line, there is a difference between the two mentioned values. This diagram provides a visual measure to evaluate the accuracy of the proposed method.

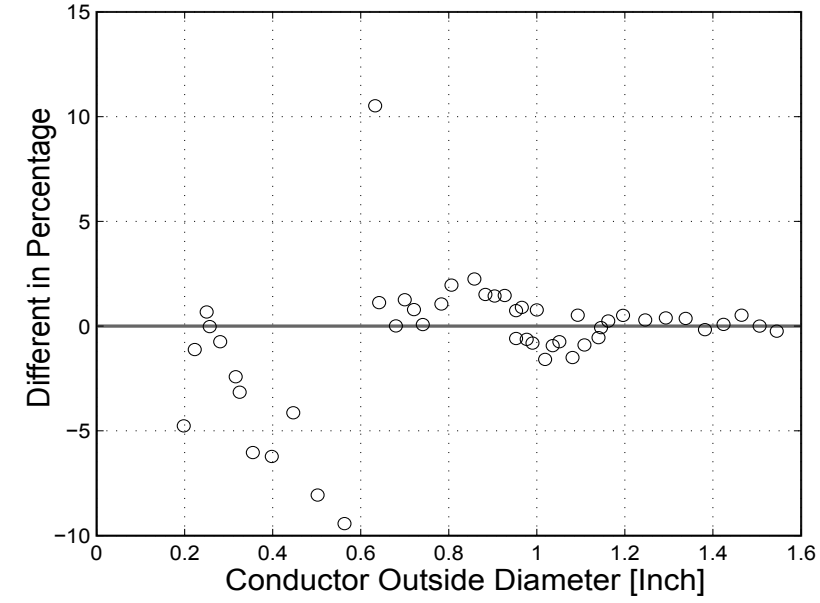

Figure 3.16: Error percentages of Ampacities for different types of conductors vs. Conductor Diameter [Inch]

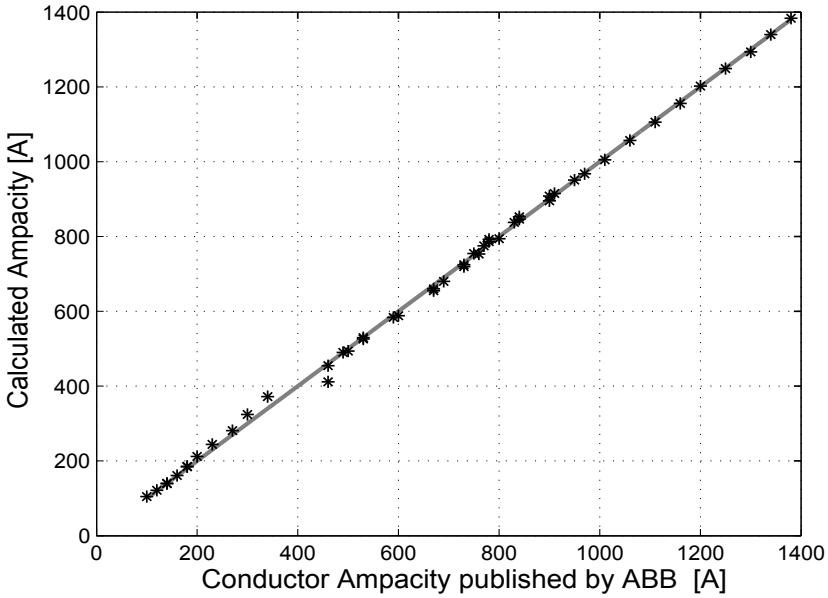

Figure 3.17: Calculated Ampacities vs. published Ampacities for different types of conductors published by Westinghouse

3.5 Thermal Rating using Numerical Weather Prediction

As the installation of monitoring stations requires a large investment, they are usually positioned at only a few locations along the line. Also, monitoring stations have challenges in dealing with maintenance and operational problems. Even if all the required sensor and monitoring equipment are installed, as the meteorological conditions change along the line, capturing the lowest value of ampacity using conventional DTR methods is infeasible [38]. Thus, having an accurate direct dynamic line rating is not possible in most cases. Therefore, the Numerical Weather Prediction (NWP) systems can be used as alternatives to online methods.

NWP is a technique to forecast weather conditions by solving a numerical model of the atmosphere for a designated area. NWP systems require access to geographical data of the terrain and meteorological initial and boundary conditions of the area under study. A high resolution NWP is able to provide weather predictions for each segment of the power transmission line with acceptable accuracy. By solving the model using numerical calculation methods, the state of each meteorological variable (such as temperature, air pressure, precipitation, moisture, and wind), can be found. NWP models are of different types and scales.

One category of NWP models used frequently is called mesoscale model. DTR systems can take advantage of these systems because they need relatively less computational processing power and can be executed on a normal computer with average performance. In this manner, the DTR system incorporates generated results of a mesoscale NWP model and uses the predicted values of meteorological parameters along the overhead lines with the required spatial resolution for accurate rating. In

addition, the overall costs of the system would be significantly less than the online systems.

Due to the fact that each segment of a transmission line might have specific ampacity, which usually is not the same as the others, the ampacity of the whole transmission line depends on the thermal ratings of the bottleneck segment. A bottleneck segment is defined as the segment with the lowest value of thermal rating. The method which is used in the current research uses this approach to calculate the ampacity of the entire line. Using the current model, a detailed examination of the power losses, which are temperature-dependent, is also performed.

3.6 Spatial Variability Analysis

Every long power transmission line is comprised of a number of spans. As the weather conditions along the line change from one span to another, the unit ampacity and resistance differ as well. In order to calculate an ampacity value which can be applied to the entire transmission line, the resistance and ampacity values of each segment must be considered. In this section the spatial variability of values is studied in detail.

The case study, the simplified power transmission network of Newfoundland and Labrador, is described in detail in chapter 5. The transmission line that is analysed in this section is the line #32. It starts from the Bay d'Espoir generating station and ends at the Holyrood thermal power plant. Specifications of this line are provided in table 5.3. This transmission line transfers the power that is generated by the hydro power plant to the next substation near the Holyrood thermal plant. The power is then transferred to the demand node through a higher capacity transmission

line, #21.

As line #21 has more ampacity and its length is only 28 kilometers, its resistance has a negligible effect on the transmission losses of the entire system. On the other hand, as line #32 has less capacity, its resistance is higher and is ten times longer than the other line; therefore, this line imposes more losses on the transmission system. For these mentioned reasons, only line #32 is analysed in this section.

Figure 3.18 shows the details of 13 segments of line #32. As the segmentation is based on the rule that each part should contain a straight line, the line segments do not have the same length.

3.6.1 Ampacity

In order to calculate the dynamic ampacity of the transmission line, the ampacity of each segment must be calculated. Based on the ampacity values of all segments, the bottleneck segment with minimum rating can be determined. The bottleneck segment determines the ampacity of the entire transmission line, which will not overload any segment. The statistical characteristics of the ampacity of each segment are described in the three following figures. The data is calculated based on the simulation period of one year, 2006. Each simulation step is 1 hour, which results in the total simulation samples of 8760.

Figure 3.19 shows the statistical data of Line #32 segment ampacities. The statistical data are demonstrated in the form of a box plot. Each box, representing a segment, shows minimum, lower quartile, median, upper quartile, and largest ampacity of the segment. The figure indicates that the seventh segment has the highest ampacity. Segment 13 has the minimum ampacity of 733.7 A and segment 7 has the maximum ampacity of 3198.7 A.

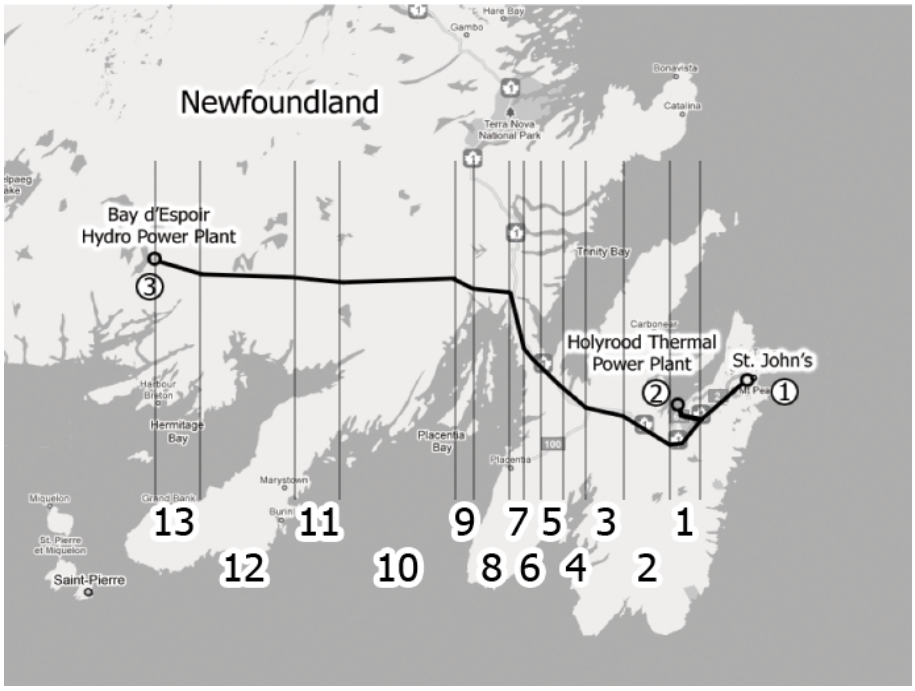

Figure 3.18: Case study power transmission network schematic, including Line #32 segment details

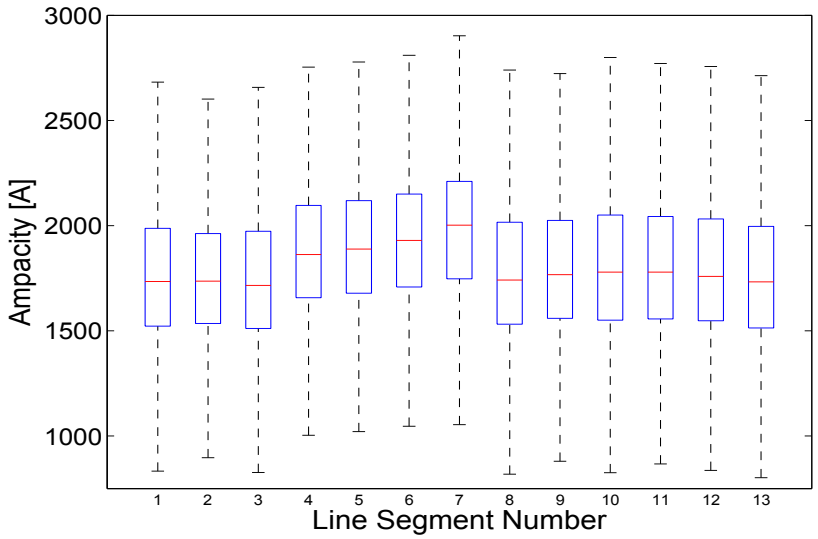

Figure 3.19: Statistical parameters of ampacity each segment of line #32

Figure 3.20 shows the histogram of ampacity difference between maximum and minimum values of line #32 at each simulation step. The graph indicates that the ampacity difference between maximum and minimum starts from very small values close to 100 A, which indicates the transmission line has a uniform ampacity in that simulation step. In some cases the ampacity difference reaches to a maximum value close to 1300 A. Higher values of ampacity difference indicate a significant change in weather conditions along this 260 kilometer line. Based on the simulation results, the expected value of difference between maximum and minimum ampacity is 600.5 A, and the expected value of ampacity of the entire line is 1500.3 A.

The histograms in Figure 3.21 show the frequency for which each segment has the maximum/minimum ampacity of the entire transmission line. In addition, the minimum value is equal to the bottleneck of the line and defines the ampacity of the whole line as well. According to the figure, the segment which is subject to worst weather conditions and therefore has the minimum ampacity majority of the time is segment #1. This segment is located beside the Holyrood thermal power plant. In addition, the figure also shows that the seventh segment has the highest ampacity most of the time, which confirms the results of the previous figure regarding the highest ampacity value.

3.6.2 Temperature

In this subsection the temperature variations of the transmission line, which are subjected to a constant current, are analysed. Study of temperature variations provides a measure to experiment whether the calculated ampacity values are appropriate. The simulations in this subsection are based on a constant current of 900 A. Figure 3.22 shows the statistical characteristics of the temperature of the segments

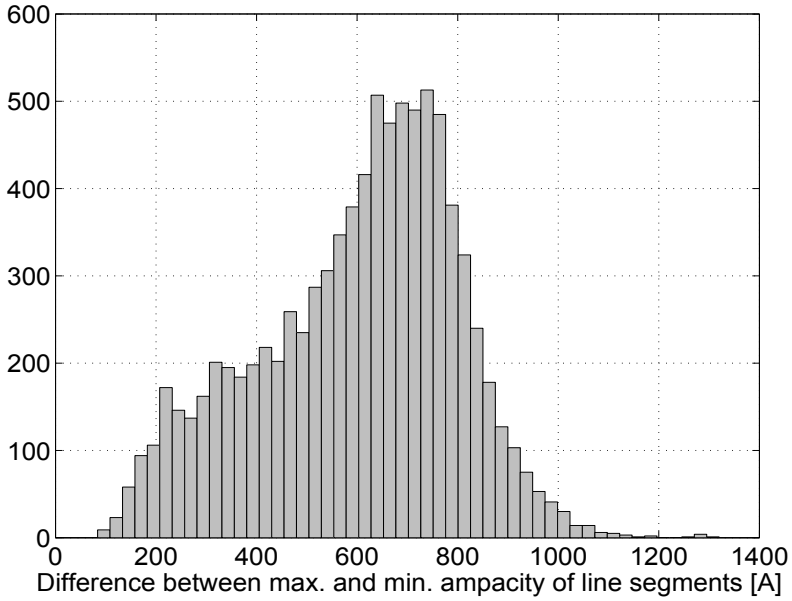

Figure 3.20: Histogram of ampacity difference between the maximum and minimum ampacity values of line #32

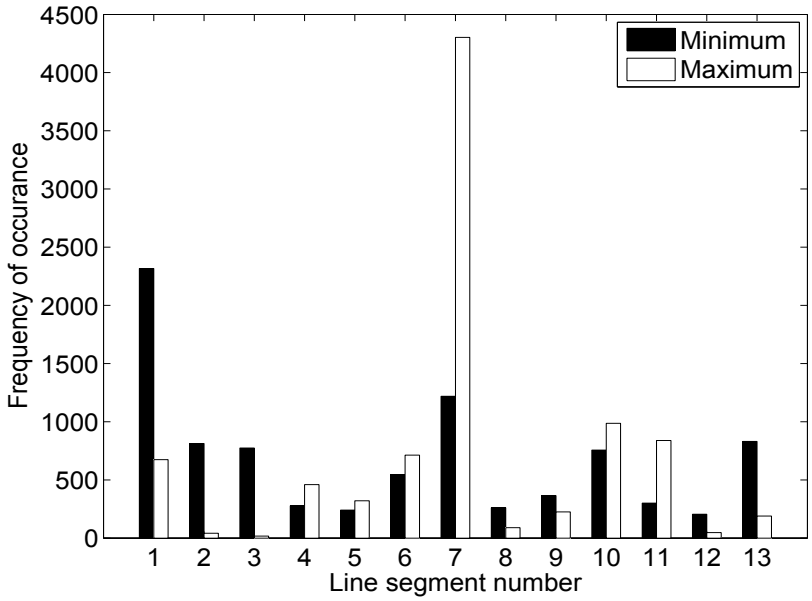

Figure 3.21: Histogram indicating the frequency of each segment having maximum/minimum ampacity

of line #32. These data are demonstrated in the form of a box plot. Each box, representing a segment, shows minimum, lower quartile, median, upper quartile, and largest temperature of the segment. The figure indicates that the seventh segment has the lowest temperature, segment 13 has the maximum temperature of 98°C, and segment 7 has the minimum temperature of -8.5°C.

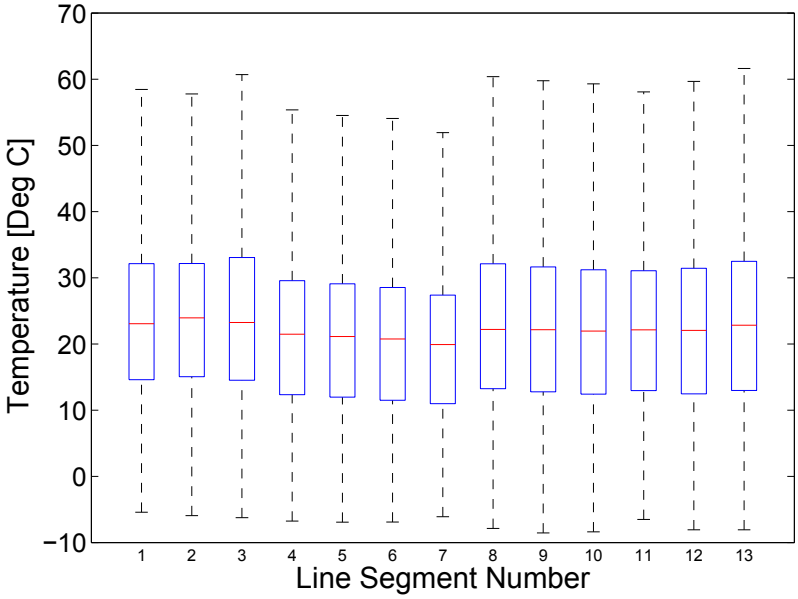

Figure 3.22: Statistical parameters of temperature each segment of line #32

Figure 3.23 shows the histogram of temperature difference between maximum and minimum values of line #32 at each simulation step. The graph indicates that the temperature difference starts from very small values close to zero, which indicates the transmission line has a uniform temperature in that simulation step. In some cases, the temperature reaches a maximum value close to 70°C. Higher values of temperature difference indicate a significant change of weather conditions along this 260 kilometer line. Based on the simulation results the expected value of ampacity

of the entire line is $22.3°C$.

The histograms in Figure 3.24 show the frequency for which each segment has the maximum/minimum temperature of the entire transmission line. In addition, the maximum value is equal to the bottleneck of the line and defines the ampacity of the whole line. According to the figure, the segment which is subject to worst weather conditions and therefore has the maximum temperature majority of the simulation steps is segment #1, which is located beside the Holyrood thermal power plant. The figure also shows that the seventh segment has the lowest temperature of most of the simulation steps. This outcome confirms the previous figure results regarding the lowest temperature and the previous subsection results.

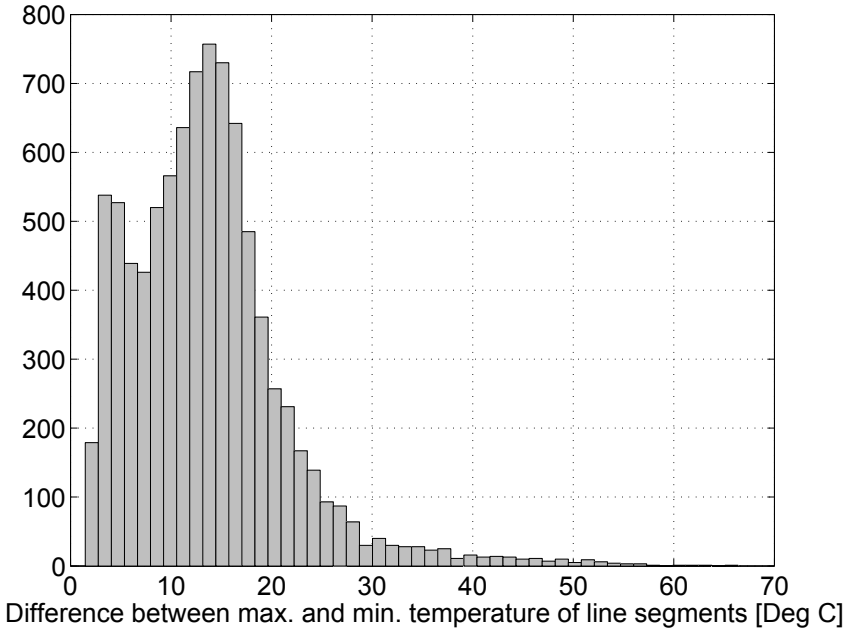

Figure 3.23: Histogram of temperature difference between the maximum and minimum temperature values of line #32

3.6.3 Resistance Calculation

There are several methods that can be used to approximate the conductor resistance. Each method has different characteristics and results. Figure 3.25 shows the results of calculating the resistance of the conductor based on the two methods incorporated in this study: Bottleneck resistance calculation and Segment by segment resistance calculation. The first method uses a bottleneck segment as a reference to calculate the resistance. The per unit resistance of the bottleneck segment is calculated based on its current. Afterwards, this per unit resistance is used for the other segments of the transmission line.

The next method, which calculates the resistance with better accuracy, is the segment by segment resistance calculation. Compared to the other segments of the transmission line, the bottleneck segment is subject to worst weather conditions and its temperature is the maximum. The maximum temperature in turn leads to maximum conductor resistance in the bottleneck segment. Therefore, the resistance of the bottleneck segment is the highest in comparison to other spans. Using this value as the unit resistance of the entire line results in higher resistance. This method calculates the resistance of each segment based on the current that is passing through it and ambient weather conditions. Afterwards the resistance values of segments are summed up to calculate resistance of the entire transmission line.

In order to compare the results of these two methods the resistance of a sample transmission line is calculated using both methods. The results are provided in Figure 3.25. The power transmission line used in this example is line #31 in Table 5.3. The simulation time is seven days and it can be seen that the bottleneck resistance method calculates the resistance with a 1.1 Ω offset. In addition, short transient

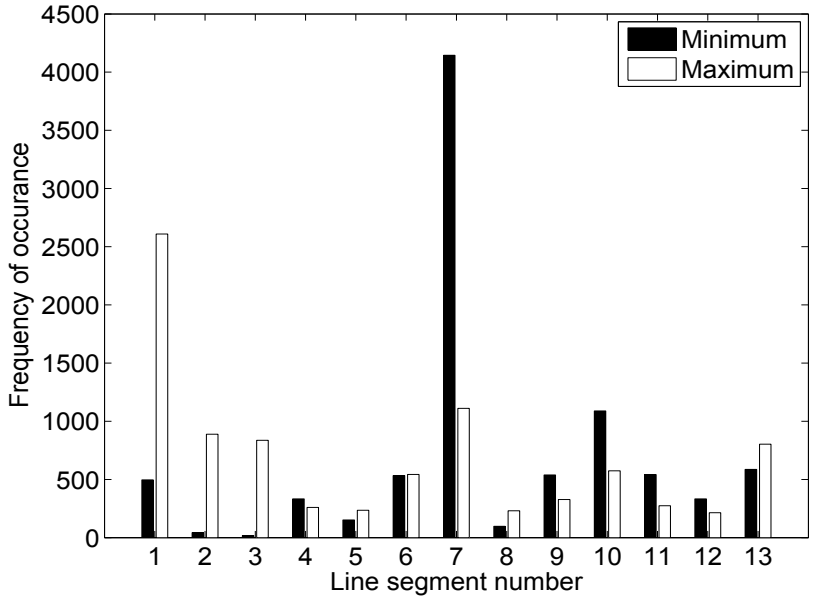

Figure 3.24: Histogram indicating the frequency of each segment having maximum/minimum temperature

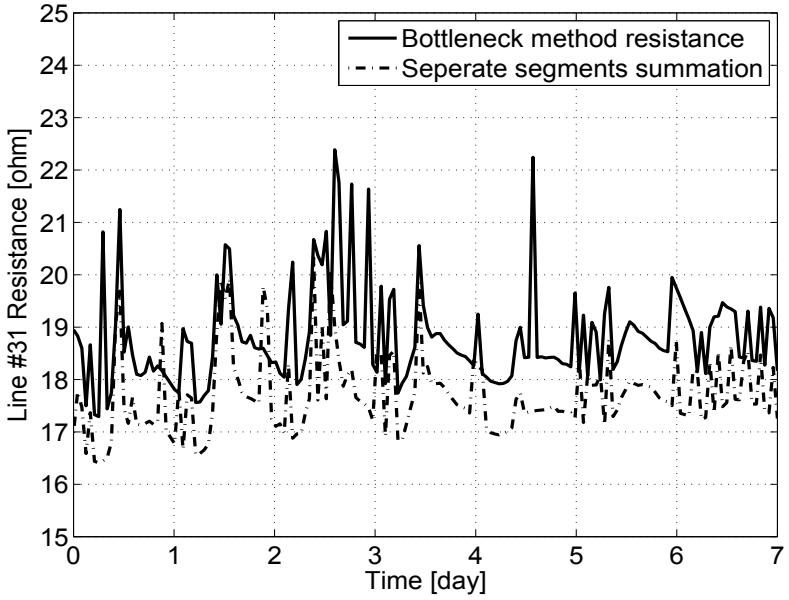

Figure 3.25: Comparison of two methods for calculating line resistance: Bottleneck and Segment by Segment methods. Bottleneck Resistance = 18.81 Ω, Separate segment resistance = 17.70 Ω

spikes present in this method are suppressed in the segment by segment method.

Chapter 4

Extensions to Economic Dispatch Problem

This chapter presents three major features and extensions of the current model. The first feature incorporates DTR as a means of increasing the ampacity of transmission lines. As explained in section 3.3, DTR requires constant monitoring and access to weather information along the line. Some of the methods described in [28] use online sensors to access this information [28]. The accuracy of these systems is better in comparison with the ones without access to online weather information. The issue with such systems is the cost of sensors and data infrastructure for transferring readings to the control centre. The second extension, a spatially resolved thermal model of the geographical area containing the transmission network, solves the problem of lack of online sensors. The thermal model uses bottleneck thermal rating method with variable locations to calculate the temperature dependent resistance of the lines. The calculated resistance allows to both estimate the ampacity of the power transmission network and represent the power losses of the network more precisely.

The third feature of the optimization model is the Multi-snapshot simulation. This feature uses the current available forecasts of line ampacity and power demand to calculate the generation share of each generator. Knowing the required power generation of each generator in advance will provide a way to cope with the thermal generator's constraint, generator start-up/shut-down delay. The following two subsections provide descriptions of the first two features of the model. Section 4.6 illustrates the multi-snapshot simulation with its mathematical rules.

4.1 Generator Cost Model

In order to model a generator in a power transmission network, several aspects must be formulated such as cost function, generation boundaries, generation ramp up/down rates. In this section the cost model of a generator is described in detail [39]. *Capital cost* is defined as the expense of land, buildings, and equipment together with generator related cost of design, planning, and installation. As this cost is considered prior to building the power plant, it is customary to amortize it over the lifespan of the power plant.

Variable and fixed costs are two parts of the *Operation and management cost*. The *variable cost* is defined as the cost of fuel and its transportation and handling along with the storage charges. As this cost is directly affected by fuel, it is also a function of generation. On the contrary, the other important part of the maintenance cost, *fixed cost*, is not dependent on the plant's generation. As long as the generator remains in an active or stand-by state this cost will exist. Therefore, fixed costs are usually normalized to the amount of generation and expressed as a monthly charge. For information on costs associated with different generation technologies, see [13],

[40], [41], [42], and [43].

Start-up costs are defined for a number of generator types such as thermal power plants [44]. The start-up cost is incurred when a generating unit transits from the "off" to "on" state. This cost is an exponential function of the duration that the plant has been off

$$CS_i\big(X_i^{\text{off}}(t)\big) = \alpha_i + \beta_i \left[1 - e^{\frac{-X_i^{\text{off}}(t)}{\tau_i}}\right]. \tag{4.1}$$

The time constant, τ_i, is a parameter of the i-th generator start-up function. X_i^{off} is the duration of the generator off-state when it restarts. Constants α_i and β_i are the parameters which depend on the mechanical and electrical characteristics of the generator.

Table 4.1 compares the general cost values for several generators [45]. According to the table, hydro power plants have the highest value of capital cost which depends on the geographical location of the plant and its construction. However, as there is no fuel cost for this plant, the generation cost will be much lower than for the other types of generation. Oil, Liquid Natural Gas (LNG), and Coal power plants are categorized as thermal plants and have relatively comparable costs. The table also indicates the various costs of two types of nuclear power plants: the Pressurized Water Reactor (PWR) and the Pressurized Heavy Water Reactor (PHWR). The capital cost of the nuclear plants is relatively higher than the other types of thermal plants; however, as the fuel costs of this plant are very low compared to fossil-fuel-burning plants, the generation cost is lower. Another important parameter for a power plant is the Forced Outage Rate (FOR) which is mentioned in the table as well.

Table 4.1: Comparison of the general cost values for different types of conductors

Plant Type	Capital Cost [$/kW]	Fixed Cost [$/(kW.Month)]	Fuel Cost [$/kWh]	FOR %	Life Time
Hydro	Highest, Variable	˜5	N/A	Variable	40˜50
Oil	812.5	2.13˜2.25	0.021˜0.030	6˜7	25
LNG	500	0.9˜2.0	0.035˜0.043	10˜11	20
Coal	1062.5	2.75˜2.81	0.014˜0.023	8.5˜9.5	25
Nuclear PWR	1625.0	4.6˜4.94	0.004˜0.005	9.0	25
Nuclear PHWR	1750.0	5.5	0.003	7.0	25

4.2 Power Generation Parameters

Describing a power generation unit using a system of mathematical equations requires approximating certain features and characteristics as mathematical relations and parameters. These are provided in the following section. Parameters *ramp-up*, RU_i, and *ramp-down*, RD_i, restrict the generation increase and decrease rates. The limiting factors are only defined for certain types of generators; for example, thermal plants that burn fuel gas, coal, and oil are in this category [42].

Power plants generally house several generating units. In order to cope with planned/forced outages and increase their safety margin, usually a single unit operates in standby mode and is called the *Spinning Reserve* [46]. Another constraint related to the thermal power plants is *Up/Down time*. For transition of a thermal unit from committed to de-committed or vice versa, the current state of the generator must be retained for a minimum time which is known as up/down time [44].

4.3 Voltage Drop Limitations

Voltage control is an important factor for power transmission systems, especially for long-distance transmission. There are several factors which alter the voltage drop level of a transmission line. Most of the factors are of a passive nature, e.g. shunt capacitance and series inductance of the transmission line. In addition, temperature variations of the series reactance are insignificant and can be neglected [47]. On a specific transmission line, the voltage level might drop or rise depending on the reactive and real parts of the power flow. Voltage level reductions of more than 5%, or in some extreme cases 10%, are not desirable [48]. For this reason, the proposed model considers voltage drop constraint at each transmission node to avoid excessive voltage drops. Generally, by increasing the length of a power transmission line the amount of flow that is required for saturating a certain line will decrease [49].

4.4 MIP Model Nomenclature

To minimize the costs of the power generation and transmission system using the ED approach, mixed integer programming (MIP) is employed in the proposed model. The MIP based model is implemented using the AMPL modeling language and contains a set of constraints and one optimization function [50]. The rest of this subsection introduces functionality of the constraints and optimization function in detail.

Optimization Function is defined as a way to minimize the total cost of power generation, including hydro and thermal power plants, while providing sufficient power for the demand node(s) in the network continuously. Figure 4.1 shows it as part of the AMPL model as well.

Power Generation Boundary; each generator has a limited range of generation capacity. This constraint defines the minimum and maximum boundaries. The thermal power plant has a complex generation profile, generally a semi-discrete characteristic which can either be zero or start producing power from the minimum generation amount. It is a reasonable argument that in reality the plant's generation cannot jump from zero to its minimum. The answer is that the cost of generating power below the minimum generation limit is as high as the minimum itself, and for the generation amounts more than a minimum, it will rise continuously and linearly. Therefore, it is usually not financially justifiable to generate power below the minimum amount. Still, the mathematical formulation of the model must be capable of assigning generation values less than the minimum when necessary. This characteristic of the thermal power plant is also implemented using the provided constraint.

As described in Section 4.2, the thermal plant requires a start signal ahead of time. The multi-snapshot simulation used in this study enables the model to send the thermal generator's early start-up/shut-down signals in advance. The *Power Generation Boundary* constraint is designed to ensure that the model works accordingly.

Generation/Demand Equilibrium and *Loss Calculation*; in a power generation and transmission system, the total generated power is equal to the demand added to the power transmission losses in the network. Generation/Demand Equilibrium constraint ensures this equilibrium remains valid. In addition, loss in a transmission line is a function of the current flowing through the line, its resistance, and the transmission line's length. The line's resistance is also a function of both the local weather conditions and the current that is passing through it. *Loss Calculation* set of constraints, by using a piecewise implementation of the nonlinear resistance, calculates the losses of the transmission line as a function of the power flowing through it.

Power Bus Flow Balance and *Network Physical Structure*; in order to simulate the minimum cost flow network for a power transmission circuit, the flow of the power into a node and the flow out of it must be in balance. In addition, each node of the transmission network might include a source/sink of power such as generator/demand. While considering all flows associated with a node, the losses of the power transmission line should be considered as well. The *Power Bus Flow Balance* constraint aids the model to calculate the power flow values strictly based on the described rule. Along with it, the *Network Physical Structure* restricts the model to route the power through existing physical transmission lines.

Line Ampacity; there are different methods to calculate the thermal rating of a transmission line. However, disregarding the rating method which the model is using, the line's ampacity during one simulation period remains constant and is defined using the rating method library. The *Line Ampacity* constraint is included to impose maximum rating or ampacity of the transmission lines. The DTR calculated ampacity of the line in this study is calculated based on the minimum DTR ampacity of different segments of that transmission line.

Ramp Up/Down; because of the mechanical characteristics of a thermal plant, the increasing or decreasing generation rate is more limited in comparison with hydro generators. Constraint *Ramp Up/Down* keeps the changing rate under control.

Voltage Drop; as discussed in section 4.3 the voltage level should remain above 5% or 10% of the generator's end of the line. The *Voltage Drop* constraint imposes this limit, which is especially important for long transmission lines.

Piecewise Linear Conversion Set; while nonlinear functions are used in modeling such as transmission losses, line temperature, and voltage drop the model must remain linear. Piecewise linear conversion is used to convert convex non-linear functions

to convex piecewise linear functions suitable for use in an MIP linear model. The *Piecewise Linear Conversion Set* constraints are defined to determine the output values of the piecewise linear function based on the input value.

4.4.1 Constants and Variables of MIP model

Constant and variable parameters which are used to define the network model are defined in tables 4.2 and 4.3 respectively.

Table 4.2: Constant parameters used in the MIP model

Parameter	Description
Δt	Simulation time step length [min]
$A_{i,j}(u)$	Ampacity of the line between buses i and j at snapshot step u [A]
$C\_Prv_i(u)$	Binary state of generator i at snapshot step u
CF_i	Fixed cost of generator located at bus i [$/min]
$D_{i,j}$	Length of line between buses i and j [km]
$DS_{i,j,k}$	Length of the k-th line segment of transmission line between buses i and j
F	Number of snapshots that the start/stop command for the thermal generator must be initialized
$ITab_{i,j}(u,k)$	An array of constant numbers that form the input data space (line current), of the piecewise lookup table
M	A large number used in the MIP Model
N	Number of buses in the network
$NS_{i,j}$	Number of transmission line segments between buses i and j
$PD_i(u)$	Power demand at bus i at snapshot step u [MW]
$PF_i(u)$	Power factor of the load at demand node i at snapshot step u
$PG_i^{\min}(u)$	Minimal allowed generation at bus i at snapshot step u [MW]
$PH_{i,j}$	Binary constant indicating electrical state of connection between buses i and j
$R_{i,j}(u)$	Resistance of the line between buses i and j at snapshot step u [Ω/km]
$r_{k,i,j}(u)$	Unit resistance of the line calculated at segment k of line between buses i and j at snapshot step u [Ω/km]
RU_i, RD_i	Ramp-up/down limit of the generator located at bus i [MW/h]
t	The current time of the simulation's first snapshot
T	The maximum simulation period
$T_{i,j}(u)$	Temperature of the line between buses i and j at snapshot step u [$^\circ K$]
$TTab_{i,j}(u,k)$	An array of constant numbers that form the output data space (line temperature), of the piecewise lookup table.
U	Number of snapshots in each simulation step

Table 4.3: Variable parameters used in the MIP model

Parameter	Description
i, j, k	Variables defined to indicate bus numbers
$C(u)$	Total cost of the power generation at snapshot step u [$]
$C\_Pres_i(u)$	Binary variable defining the availability state of generator i
$CS_i(u)$	Start-up cost associated with generating unit i at time step u [$]
CV_i	Variable cost coefficient of generator i [$/MW]
$I_{i,j}(u)$	Current flowing through the line between buses i and j at snapshot step u [A]
$L(t)$	Power loss of the entire network [MW]
$L_{i,j}(u)$	Power loss of the line between buses i and j at snapshot step u [MW]
$PFL_{i,j}(u)$	Power flow through the line between buses i and j at snapshot step u [MW]
$PG(u)$	Total power generated at snapshot step u [MW]
$PG_{i,supp}(u)$	Supplementary power generation variable at bus i at snapshot step u [MW]
$PG_i(u)$	Power generation at bus i at snapshot step u [MW]
$PG_i^{\max}(u)$	Maximum allowed generation at bus i at snapshot step u [MW]
$PG_i^{\min}(u)$	Minimum allowed generation at bus i at snapshot step u [MW]
PS	Variable used for linear approximation in piecewise function's lookup table
PZ	Binary variable used for linear approximation in piecewise function's lookup table
$V_i(u)$	Voltage level at node i [V]
$Z(t)$	Total generation cost of the system [$]

4.5 MIP Model Structure

Figure 4.1 shows a block diagram of the optimization model developed in this study. It is divided into four major subdivisions: Inputs, the main program which is written in C++, the AMPL mathematical model for optimization, and Outputs.

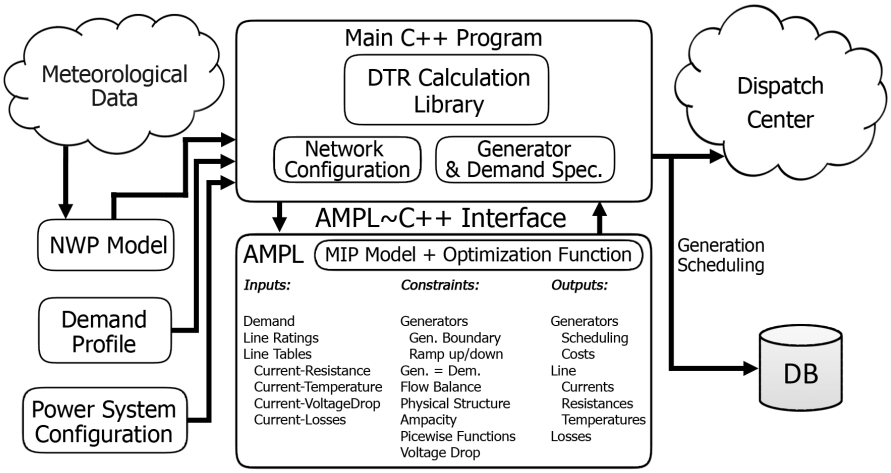

Figure 4.1: A Block diagram of the optimization model

System inputs include meteorological data, demand profile, and the power system configuration. As mentioned in subsections 5.1.2 and 5.1.1, the weather data related to the power transmission network are acquired from the NARR dataset [51], the demand profile is synthesized using a typical weekly load profile from [26] and statistics of weekly consumption data. The transmission network and power generators' configuration are initialized at the start and remain constant throughout the simulation.

The main C++ program is responsible for providing the input data for the AMPL core in its specific format. Using the mathematical model defined in AMPL, the required generation shares and outputs are calculated in AMPL. The results are

returned back to the C++ program and stored into the database.

4.6 MIP Model Description

The optimization function, described below, formulates the goal of the model: to minimize the generation costs of the power transmission network.

$$Z(t) = \min \sum_{u=t+1}^{t+U} \sum_{i=1}^{N} \left[CF_i \times \Delta t + CV_i \times PG_i(u) + CS_i(u) \right]. \tag{4.2}$$

To be able to calculate the predicted values for demand and weather conditions, the model requires that each simulation step contain several snapshots. While the first snapshot contains the data for the current simulation, the remaining snapshots represent the status of demand and network capacity in the following hours.

Parameter U specifies the number of snapshots which should be processed in each simulation step. Consider an example where parameter U is equal to six hours. The simulator considers the current demands and network capacity with the data for the remaining five hours. For simplicity, the simulation time, t, is assumed to be equal to 1 in the following equations. The minimum and maximum generation limit of each power plant, at snapshot step u, are described using *Power Generation Boundary*

$$PG_i(u) \leq C\_Pres_i(u) \times PG_i^{max}(u) \quad \forall i \in N, \quad u \in [1, U] \tag{4.3}$$

$$PG_i(u) - PG_i^{min}(u) \leq PG_{i,supp}(u) \quad u \in [1, F] \tag{4.4}$$

$$C\_Pres_i(u) = C\_Prv_i(u) \quad \forall i \in N, \quad u \in [1, F] \tag{4.5}$$

Equation (4.3) is designed to ensure that the generation amount of each plant remains within the boundaries. It keeps the generator model from operating in invalid generation modes, such as negative or overcapacity generation. Parameter $C\_Pres_i(u)$ puts the generator in the standby or generation mode when its value is equal to 0 or 1, respectively. The parameter $PG_{2,supp}$, is an auxiliary variable, defined to indicate the amount of generation above the thermal power plant's minimum generation. The spinning reserve power can be included in the generator's maximum limit parameter, $PG_i^{max}(u)$.

As the simulation advances, the MIP model's decision regarding the generation states of the thermal generator must remain fixed so they can be applied to the power plants. Parameter F is the limit for converting these results to constants. While it is possible to change a generator's state in the snapshot $f+1$, the same state will become constant in snapshot f and lower. Parameters C_Prv_i and C_Pres_i are used to implement this requirement in the model. Equation (4.5) expresses this feature.

In each simulation step, the generation/demand equilibrium of all snapshots is ensured by the following constraint

$$\sum_{i=1}^{N} PG_i(u) = \sum_{i=1}^{N} \frac{PD_i(u)}{PF_i} + \sum_{i=1}^{N}\sum_{j=1}^{N} L_{i,j}(u) \quad \forall u \in U \tag{4.6}$$

The following equation formulates the line resistance calculation constraint

$$L_{i,j}(u) = R_{i,j}\left(I_{i,j}(u)\right) \times I_{i,j}^2(u) \quad \forall (i,j) \in (N,N), \forall u \in U \tag{4.7}$$

As described in subsection 4.6, this is a non-linear convex function. Therefore, it is necessary to use an approximation method such as piecewise linearization, to preserve the linearity of the model. Piecewise linearization approximates both terms of the

equation.

The *Power Bus Flow Balance* constraint guarantees that the sum of the generated and incoming power at the snapshot u at node i is equivalent to the sum of the power consumed at this node and the power flowing out of it (without taking losses into account). The line loss term is included only in one direction of the power flow, for instance on the right side of the equation.

$$PG_j(u) + \sum_{i=1}^{N} PFL_{i,j}(u) = \frac{PD_j(u)}{PF_j} + \sum_{k=1}^{N} \left(PFL_{j,k}(u) + L_{j,k}(u)\right). \qquad (4.8)$$
$$\forall i, j, k \in N, \quad \forall u \in U$$

The set of binary constant parameters called PH formulates the physical structure of the network. These constraints, described as the *Network Physical Structure*, force the model to route the power flow through existing paths in the network and avoids the use of virtual, non-existing paths in the transmission matrix. $PH_{i,j}$ value is set when there is an electrical connection between buses i and j. Otherwise the $PH_{i,j}$ value is set to zero.

$$PFL_{i,j}(t) \leq M \times PH_{i,j}; \quad \forall (i,j) \in (N,N). \qquad (4.9)$$

The current flow of the line is controlled using the *Line Ampacity* constraint. It guarantees that the current does not exceed the line's ampacity (calculated by either STR or DTR methods)

$$I_{i,j}(u) \leq A_{i,j}(u); \quad \forall (i,j) \in (N,N), \quad \forall u \in U \qquad (4.10)$$

Only active voltage drops of the transmission lines have considered in the current model. The *Voltage Drop* constraint is formulated as follows

$$V_i - \sqrt{3} I_{i,j} \times R_{i,j}(u) \geq V_i \times 0.95 \quad \forall i, j \in (N, N) \quad \forall u \in U \tag{4.11}$$

The last implemented constraints are the ramp-up and ramp-down generation limits modeled using the following two inequalities

$$PG_i(u) - PG_i(u-1) \leq RU_i; \quad \forall i \in N, \quad \forall u \in U \tag{4.12}$$

$$RD_i \leq PG_i(u-1) - PG_i(u); \quad \forall i \in N, \quad \forall u \in U \tag{4.13}$$

Note that to model this constraint, which is only applied to thermal power plants, specification of the initial generation amount of each plant is required. To keep the constraints consistent for all generator types, variables RU_i and RD_i are also used for hydroelectric and other types of generators without ramp-up/down limits. However, in such cases a relatively large value is assigned to the limit to virtually eliminate the constraint (e.g. maximum capacity of a generator multiplied by two).

4.7 Piecewise Linear Variable Constraints

As explained in section 4.6, to provide a solution to problems with non-linear constraints using linear programming methods, piecewise linear functions can be employed. For a complete description and formulation of piecewise functions in an MIP, refer to Chapter 17 of [50]. The non-linear variables and functions in the model, converted to piecewise linear, are: *voltage drops, transmission losses, line resistance,* and *line temperature*.

Because the resistance is a function of the temperature, it is affected by weather conditions along the line and the current passing through it [5]. To determine both

temperature and resistance of the line, a piecewise linear conversion from current to temperature/resistance at each snapshot is necessary. For resistance, this relation is described in the form of *Piecewise Linear Conversion Set* constraints

$$I_{i,j}(u) =$$

$$\sum_{k=1}^{PiecewisePoints} (ITab_{i,j}(u,k) \times PZ(u,k) + (ITab_{i,j}(u,k+1) - ITab_{i,j}(u,k)) \times PS(u,k)) \tag{4.14}$$

$$T_{i,j}(u) =$$

$$\sum_{k=1}^{PiecewisePoints} (TTab_{i,j}(u,k) \times PZ(u,k) + (TTab_{i,j}(u,k+1) - TTab_{i,j}(u,k)) \times PS(u,k)) \tag{4.15}$$

$$PS(u,k) <= PZ(u,k) \quad \forall u \in U, \quad \forall k \in PiecewisePoints \tag{4.16}$$

$$\sum_{k=1}^{PiecewisePoints} PZ(u,k) = 1, \quad \forall u \in U \tag{4.17}$$

Parameters $ITab_{i,j}(u,k)$ and $TTab_{i,j}(u,k)$ form a lookup table that maps line currents to their corresponding temperature values. Indices i and j indicate the transmission line (or span) connecting the two nodes, u specifies the current snapshot, and k is the number of linear segments that approximate the convex function. PZ is a binary variable, used with PS, to linearly approximate a particular temperature, using the respective current values. Because for any given value, only one segment of the piecewise linear approximation is used, the sum of all values of PZ in equation (4.17) is restricted to one.

Chapter 5

Simulation Study

5.1 Case study, Newfoundland and Labrador

To demonstrate the performance of the proposed method and illustrate the benefits of using DTR to solve the ED problem, the developed model was applied to a simplified power transmission network connecting two generators and a load centre in Newfoundland, Canada. The largest load centre on the island, the city of St. John's, is used as the demand node with power plants having limited generation capacity. Holyrood, the oil-burning thermal power plant is located approximately 28 kilometers from the city and covers only a portion of the demand. In addition, it produces non-renewable, expensive power. To cover the full demand, a hydro power plant located hundreds of kilometers west of the city, generates the remaining energy.

5.1.1 Transmission Network

Figure 5.1 illustrates the simplified power transmission network employed in the case study. The network includes three main buses: two power plants (Holyrood

and Bay d'Espoir) and one load centre (the city of St. John's). Table 5.1 provides the specifications of each bus.

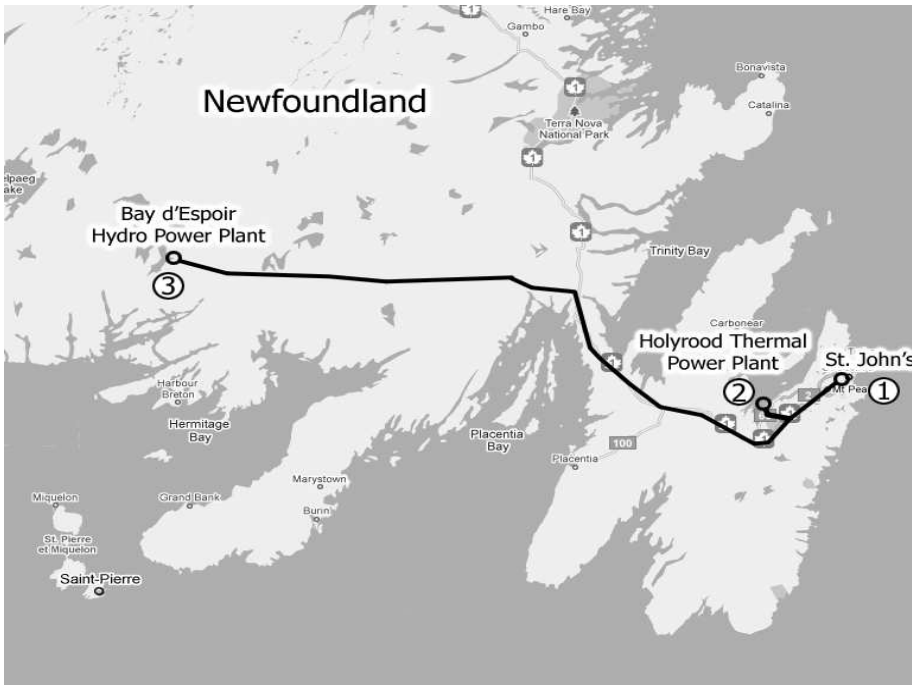

Figure 5.1: Simplified transmission network

Four main hydro power plants (Cat Arm, Hinds Lake, Upper Salmon, and Bay d'Espoir) are located in the central and north-west of Newfoundland [52]. To reduce the complexity of the model, it is assumed that the entire generation capacity of all four stations is produced by Bay d'Espoir, which is located nearly 265 kilometers west of the load centre. Bay d'Espoir, the largest hydro power plant on the island, produces 68% of the total hydroelectric energy. In addition, the remaining hydro-generated energy from the west part of the island is transmitted through this node. The spinning reserve of this station is a 150 MW unit. The same capacity is assumed for the spinning reserve of the combined generators.

Holyrood uses heavy oil as fuel for producing energy. In addition, the fuel for

Table 5.1: Generation/Demand specifications of the case study

Bus Name	St. John's	Holyrood	Bay d'Espoir
Bus #	1	2	3
Maximum Generation [MW]	0	748	330
Maximum Demand [MW]	900	0	0

the generator is delivered by ship, resulting in increased cost of generation. The maximum generation capacity of Holyrood is 330 MW and its spinning reserve is 160 MW. Table 5.2 summarizes the characteristics and cost parameters of the two generators used in this study. Reference [52] provides further information about the power generation system of the province.

Table 5.2: Assumed generator characteristics and cost parameters in case study

Generator Name	Bay d'Espoir	Holyrood
Generator type	Hydro	Thermal
Maximum Generation Capacity [MW]	898	490
Normal Generation Capacity [MW]	748	330
Spinning Reserve [MW]	150	160
Ramp Up Coeff. [MW/h]	-	110
Ramp Down Coeff. [MW/h]	-	160
Fixed Cost [k$/month]	4490	1836
Variable Cost [k$/MW]	0.00013	0.13
Start-up Time Constant [h]	-	4.0
Start-up α Constant	-	4500
Start-up β Constant	-	4500
start-up/shut-down delay [h]	-	4
# of generating units	6	2
# of standby units	1	1

Three major power transmission lines are considered in this case study. Line #31 connects Bay d'Espoir directly to St. John's. Line #32 also begins in Bay d'Espoir and extends 260 kilometers to Holyrood. Line #21 then continues from Holyrood to St. John's. These power lines are almost parallel and pass all the way through the same power transmission corridor. Table 5.3 provides the assumed characteristics of the conductors along with their nominal thermal ratings [37].

The transmission network's demand node is the city of St. John's. The variable demand of this node is simulated using a typical normalized load profile [26],

Table 5.3: Assumed transmission line characteristics in case study

Line #	Line Start	Line End	Cond. Type	Static Rating [A]	Line Length [km]
31	Bay d'Espoir	St. John's	Drake	900	265
32	Bay d'Espoir	Holyrood	Drake	900	260
21	Holyrood	St. John's	Bluebird	1751	28

and gathered statistics of the consumption (weekly average, minimum, and maximum). The statistical data used to develop the annual load profile, is illustrated in Figure 5.3. It shows the weekly average and the average of minimum and maximum values together. Using the values of minimum, maximum and average, the weekly load profile template was modulated for the entire year. The joining point between two weeks is calculated using the average of the last data point of the first week and the start point of the next week. Figure 5.2 shows an example of the weekly load profile, while Figure 5.4 presents the annual load profile.

5.1.2 Local Weather Information

To approximate real-time ampacity of the line, weather conditions along the transmission corridors must be considered. North American Regional Reanalysis (NARR) historical dataset [51] was used in this study to provide the meteorological data. The employed variables for ampacity calculations include horizontal wind speed and direction, ambient temperature, and short/long-wave radiation [53]. One year (January 1, 2006 – December 31, 2006) worth of NARR data was interpolated to the location of the power transmission corridor with a 1-hour time resolution. Local ampacity was calculated at multiple locations along the lines, and the smallest value for a particular line segment was considered as the constraining factor [54]. Comparison

of DTR vs. nominal STR is compared against dynamically determined ampacities (DTR) for a one-week simulation period of a week, in Figure 5.5 for power transmission line #31. During the sample period, DTR is greater than STR. The DTR mean value is 1304 A compared to the nominal STR of 900 A.

5.2 Static and Dynamic Thermal Rating

Normally, the static ampacity of a transmission line is lower than the DTR. To compare the two ratings, the maximum demand was set so that the required power can be transmitted using the static limit. Simulation results suggest that, in both cases, the bulk amount of power can be transmitted from the cheaper hydro power plant to the city. Because of the line ampacity restrictions, only peak demand that cannot be transferred from the hydro plant is covered by the Holyrood thermal plant. By comparing Figures 5.6 and 5.7, which show two-week samples of simulations using the two approaches, significant differences between systems using STR and DTR can be observed.

Both figures indicate the maximum power that can be dispatched from the Bay d'Espoir generator using a dotted line. The maximum generation limit is determined by the generation capacity of the hydro plant. In the DTR simulation case, maximum supply from the hydro power plant is determined only by this limitation. As for the STR case, it is limited by the line ampacity, which is less than the maximum capacity of the hydro station. On the last day of the sample simulation period, the generation at Bay d'Espoir raises more than the rated capacity. This is because of the fact that the MIP model utilized the spinning reserve for this plant to satisfy increased power demand. In the STR method, it is not possible to utilize the reserve as the ampacity is

not variable. However, using the DTR method, there is enough transmission capacity to employ this extra generation source.

The results of simulations using the two methods are provided in Table 5.4. The demand and meteorological scenario employed for both simulations correspond to the year 2006. The prediction frame window duration is 12 hours, and the maximum demand is 900 MW. Compared to STR, the total annual cost of generation has decreased by $4.37M using DTR. In addition, the thermal generator start-up count, and its share in generating energy, have decreased significantly. In general, it can be deduced that by using DTR, because of the additional transmitted power, the transmission line itself and the whole system generates higher power losses. The results also confirm this assumption: using the DTR method, the losses increase by about 15%. However, this increase is dwarfed by the savings of generation costs, which can be achieved by using DTR.

5.3 Baseload operation of hydroelectric generator

This part of the simulations is dedicated to comparing the static and dynamic thermal rating cases with the traditional method of baseloading. The simulation parameters are kept as close as possible to the configuration used in the previous section. The prediction frame window duration is 12 hours, and the maximum demand is 900 MW. The hydro power plant is selected as the baseload generator because of the lower cost of its operation. Assuming that its maximum generation capacity is 550 MW, the remaining share of the energy can be generated by the thermal power plant. The last part of the table 5.4 shows the results of this simulation.

Table 5.4: Annual and seasonal comparison of simulation results using STR, DTR, and Baseload methods.

	Annual	**Spring**	**Summer**	**Fall**	**Winter**
			Fixed Baseload Method		
Cost [M$]	145.44	28.75	19.54	34.70	62.45
Start-up Cost [K$]	1008.09	364.61	0	483.47	160.00
Generated Power [GW]	4351.28	1028.51	735.00	1127.01	1460.76
Losses [GW]	191.49	47.25	34.69	52.44	57.11
Losses/Generation %	4.40%	4.59%	4.72%	4.65%	3.91%
Maximum Demand [MW]	900.00	713.72	441.73	774.52	900.00
Hydro Gen. Share	87.92%	93.09%	100.0%	89.61%	76.88%
Thermal Gen. Share	12.08%	6.91%	0%	10.39%	23.12%
# of Start-ups	113	41	0	54	18
			Static Thermal Rating		
Cost [M$]	94.92	20.09	19.56	21.30	33.97
Start-up Cost [K$]	916.36	107.88	9.00	152.84	646.63
Generated Power [GW]	4373.85	1029.85	727.10	1131.38	1485.52
Losses [GW]	214.04	48.59	26.79	56.81	81.84
Losses/Generation %	4.89%	4.72%	3.68%	5.02%	5.51%
Maximum Demand [MW]	900.00	713.72	441.73	774.52	900.00
Hydro Gen. Share	96.82%	99.36%	99.99%	98.48%	92.25%
Thermal Gen. Share	3.18%	0.64%	0.01%	1.52%	7.75%
# of Start-ups	102	12	1	17	72
			Dynamic Thermal Rating		
Cost [M$]	90.55	19.55	19.54	20.60	30.86
Start-up Cost [K$]	728.29	35.97	0	125.88	566.44
Generated Power [GW]	4406.10	1038.07	734.10	1141.35	1492.57
Losses [GW]	246.29	56.82	33.79	66.79	88.90
Losses/Generation %	5.59%	5.47%	4.60%	5.85%	5.96%
Maximum Demand [MW]	900.00	713.72	441.73	774.52	900.00
Hydro Gen. Share	97.57%	99.71%	100.0%	98.95%	93.83%
Thermal Gen. Share	2.43%	0.29%	0%	1.05%	6.17%
# of Start-ups	81	4	0	14	63

Compared with both DTR and STR methods, using the baseload generation method results in a considerable increase of generation cost and decrease in losses. The cost has increased by 60.62% and 53.22% compared with DTR and STR, respectively. The losses decreased by 22.25% compared with DTR and 10.54% for STR. As for the thermal power plant's number of start-ups and the associated costs, the results show that there is no improvement when the baseload method is used instead of STR. However, both methods are inclined to under-utilize the full capacity of the hydro power plant and therefore need more shares of thermal generation. When compared to the STR, the baseload method decreases the share of hydro generation by 8.9%, which in turn further increases the total cost of power generation. Figure 5.8 shows a two-week sample of the baseload simulation.

5.4 Comparison of different prediction frames

The results of simulations using various prediction frame window (PFW) lengths are demonstrated in Tables 5.5, 5.6 and 5.7. For the current study, durations of 6, 9, 12, 15, 18, 24 and 36 hours have been simulated. In this set of experiments, the maximum demand of St. John's is assumed to be 900 MW for all configurations. Comparison of the costs of simulations indicates that the minimum cost is associated with the PFW length of 24 hours. However, the start-up count is minimal for 36 hours. In addition, the cost of the thermal generation, produced power, and losses are lowest in the latter case.

Figure 5.9 shows the total cost of power generation and the total simulation time, for different lengths of PFW. While increasing the duration of PFW from 6 to 36, the graph shows the time required to complete the simulations increases considerably.

Starting from small values, it continues to rise to reach the maximum of 434 hours and 35 minutes for the longest PFW. The simulation times indicate the time required to run a whole year of experiment. The total cost changes result in $1.1M annual savings, approximately 2% of the current cost. The optimal value PFW=24h needs a calculation time of less than 16 minutes a day. Figure 5.9 shows all simulation results in graphical format and table 5.8 shows them in numerical format.

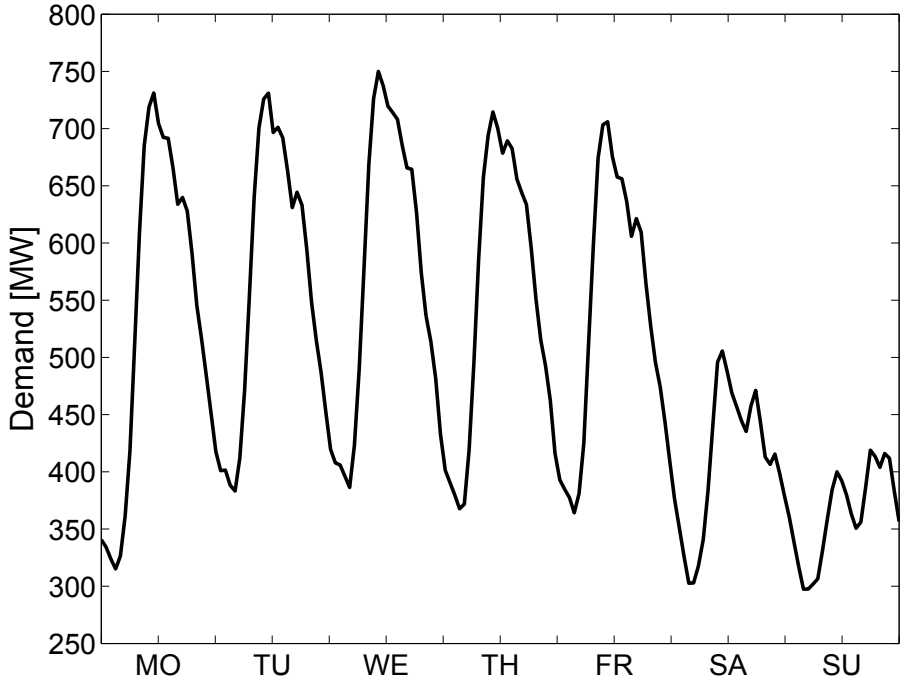

Figure 5.2: Assumed weekly load profile of St. John's

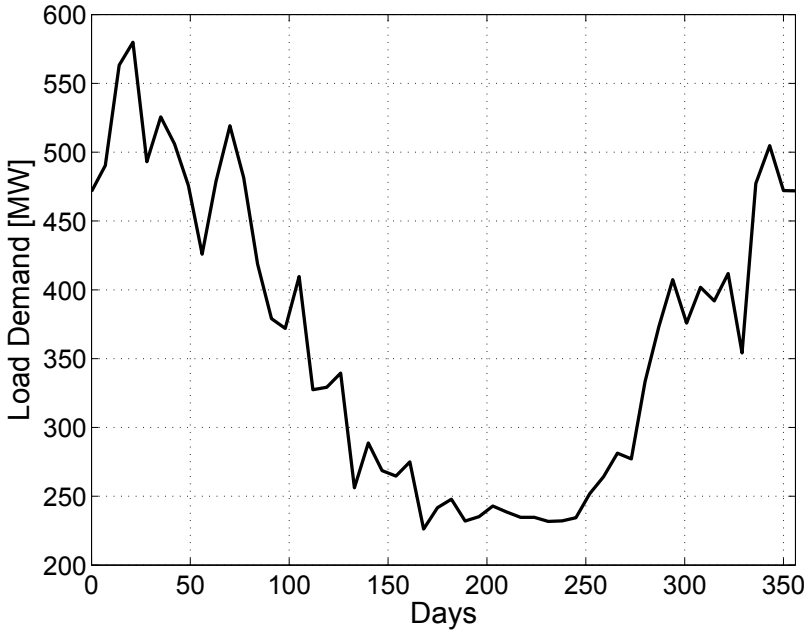

Figure 5.3: Statistical annual load information of St. John's

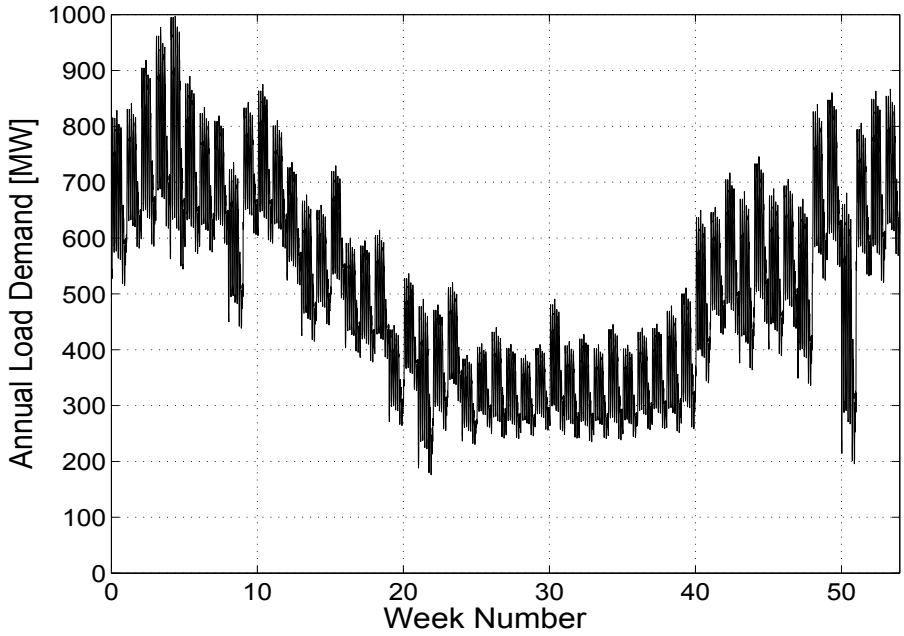

Figure 5.4: Assumed annual load profile of St. John's

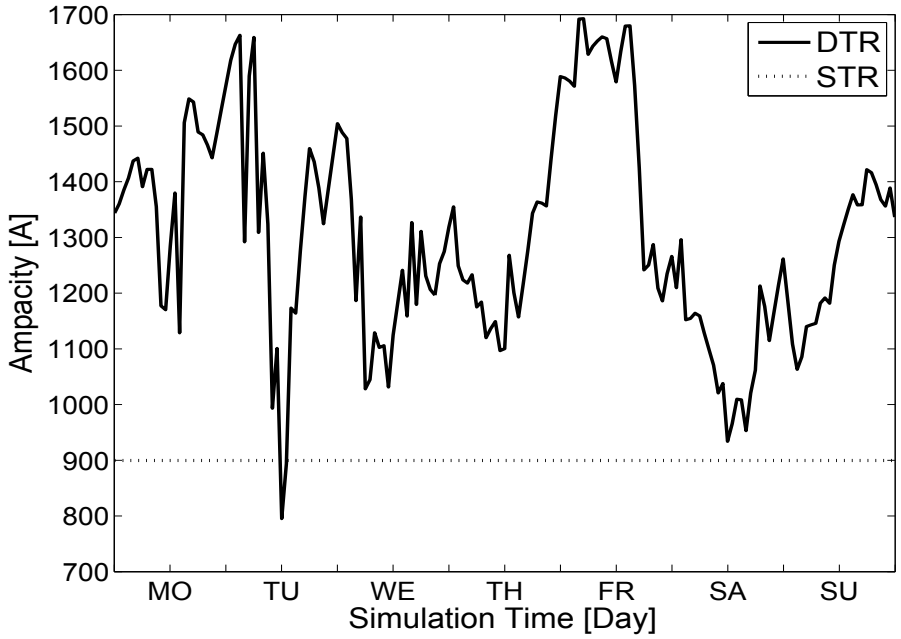

Figure 5.5: Ampacity of line #31: nominal static rating (STR) and dynamic ampacity (DTR)

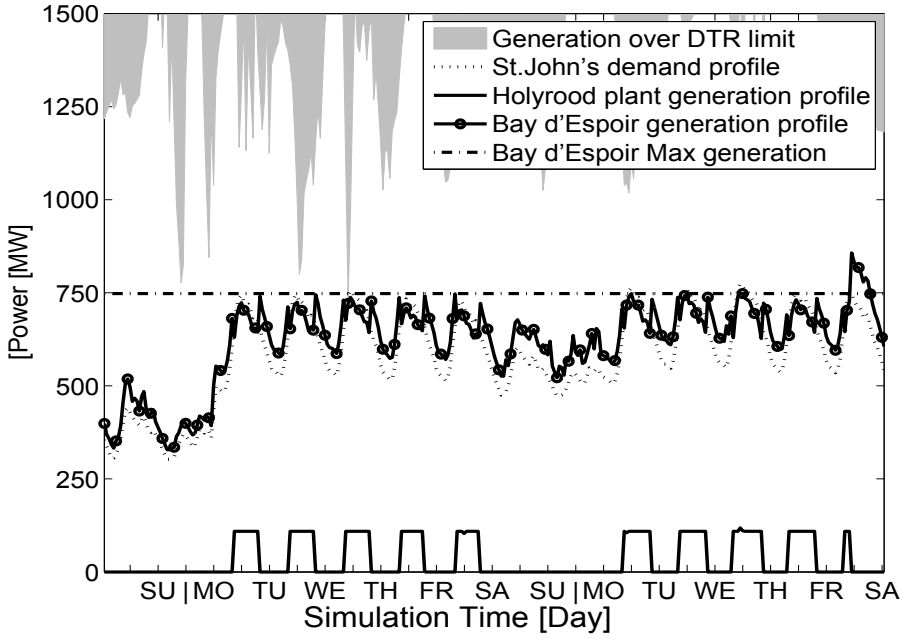

Figure 5.6: Generator scheduling results using the DTR method on a 2 week sample of load profile

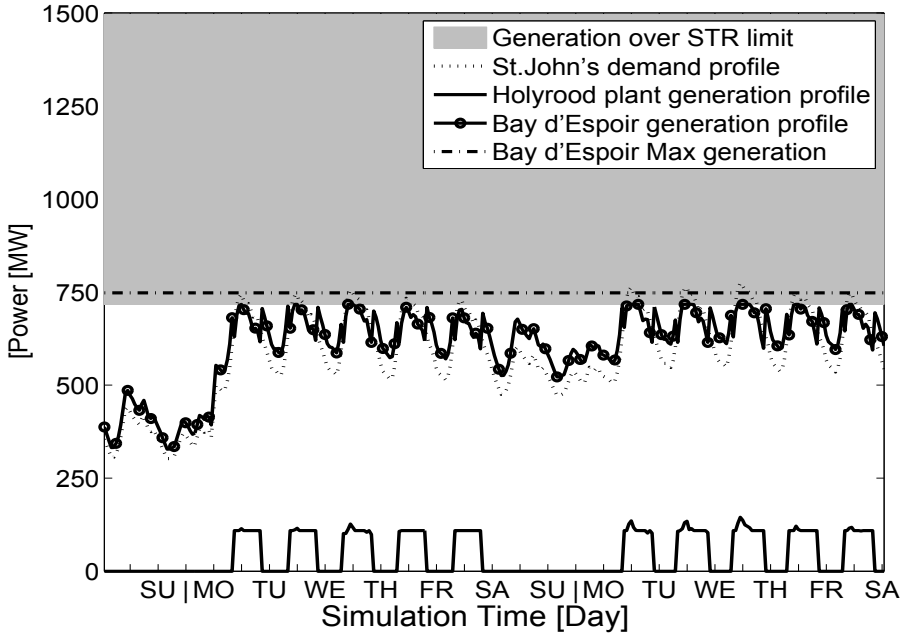

Figure 5.7: Generator scheduling results using the STR method on a 2 week sample of load profile

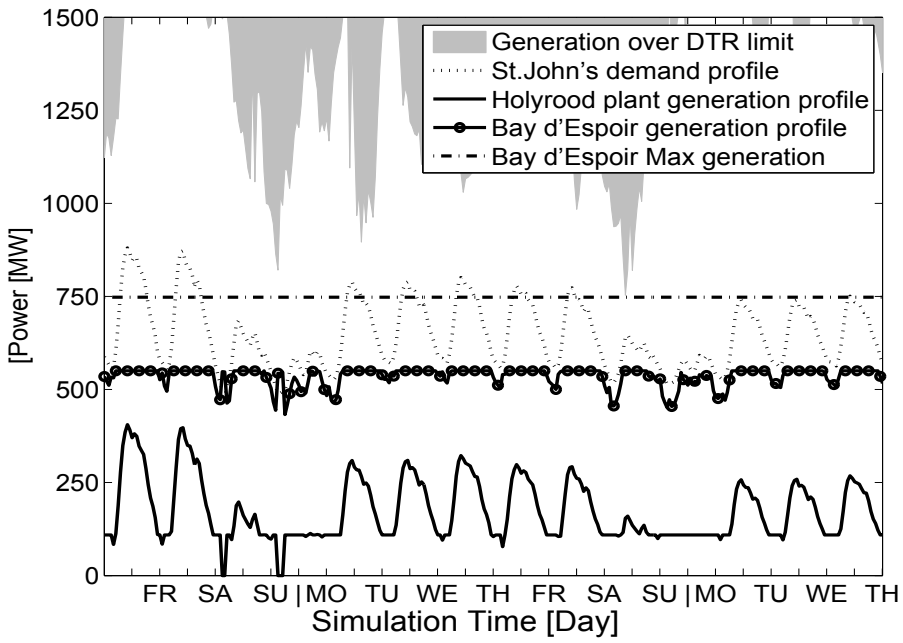

Figure 5.8: Generator scheduling results of using hydro generator as baseload of 550 MW on a 2 week sample of load profile

Table 5.5: Results of simulation using different PFW, first part

	Prediction Window [H]	Annual	Spring	Summer	Fall	Winter
Cost [M$]	6	90.68	19.55	19.54	20.61	30.98
	9	90.81	19.55	19.54	20.71	31.00
	12	90.73	19.55	19.54	20.71	30.93
	15	90.66	19.55	19.54	20.71	30.85
	18	90.71	19.55	19.54	20.72	30.90
	24	89.71	19.52	19.54	20.71	29.94
	36	89.75	19.58	19.54	20.34	30.29
Start-up Cost [K$]	6	762.33	35.97	0.0	134.88	591.48
	9	759.60	35.97	0.0	125.88	597.74
	12	753.33	35.97	0.0	125.88	591.48
	15	753.33	35.97	0.0	125.88	591.48
	18	753.33	35.97	0.0	125.88	591.48
	24	753.78	44.97	0.0	125.88	582.93
	36	741.98	35.97	0.0	106.23	599.78
Generated Power [GW]	6	4430.29	1042.77	737.98	1150.44	1499.10
	9	4413.60	1038.85	736.29	1144.56	1493.91
	12	4406.30	1037.57	734.21	1141.68	1492.84
	15	4400.86	1036.05	733.23	1139.38	1492.20
	18	4398.88	1035.12	732.96	1139.21	1491.59
	24	4401.57	1036.31	733.86	1138.42	1492.98
	36	4390.11	1034.62	733.59	1131.29	1490.62

Table 5.6: Results of simulation using different PFW, second part

	Prediction Window [H]	Annual	Spring	Summer	Fall	Winter
Losses [GW]	6	270.50	61.51	37.67	75.88	95.45
	9	253.82	57.59	35.98	70.00	90.25
	12	246.51	56.31	33.91	67.11	89.18
	15	241.08	54.79	32.92	64.82	88.55
	18	239.09	53.86	32.65	64.64	87.94
	24	241.78	55.05	33.55	63.85	89.33
	36	235.00	53.36	33.28	60.73	87.63
Losses per Generation Percentage	6	6.11%	5.90%	5.10%	6.6%	6.37%
	9	5.75%	5.54%	4.89%	6.12%	6.04%
	12	5.59%	5.43%	4.62%	5.88%	5.97%
	15	5.48%	5.29%	4.49%	5.69%	5.93%
	18	5.44%	5.20%	4.45%	5.67%	5.90%
	24	5.49%	5.31%	4.57%	5.61%	5.98%
	36	5.35%	5.16%	4.54%	5.37%	5.88%
Hydro Gen. Share	6	97.56%	99.71%	100.0%	98.96%	93.80%
	9	97.53%	99.71%	100.0%	98.88%	93.78%
	12	97.54%	99.71%	100.0%	98.87%	93.81%
	15	97.55%	99.71%	100.0%	98.87%	93.84%
	18	97.54%	99.71%	100.0%	98.87%	93.82%
	24	97.71%	99.74%	100.0%	98.87%	94.31%
	36	97.70%	99.69%	100.0%	99.10%	94.13%

Table 5.7: Results of simulation using different PFW, third part

	Prediction Window [H]	Annual	Spring	Summer	Fall	Winter
Thermal Gen. Share	6	2.44%	0.29%	0.0%	1.04%	6.20%
	9	2.47%	0.29%	0.0%	1.12%	6.22%
	12	2.46%	0.29%	0.0%	1.13%	6.19%
	15	2.45%	0.29%	0.0%	1.13%	6.16%
	18	2.46%	0.29%	0.0%	1.13%	6.18%
	24	2.29%	0.26%	0.0%	1.13%	5.69%
	36	2.30%	0.31%	0.0%	0.90%	5.87%
# of start-ups	6	85	4	0	15	66
	9	85	4	0	14	67
	12	84	4	0	14	66
	15	84	4	0	14	66
	18	84	4	0	14	66
	24	84	5	0	14	65
	36	83	4	0	12	67
Maximum Demand [MW]	6,9,12,15 18,24,36	900.0	713.72	441.73	774.52	900.0

Table 5.8: Comparison of different PFW length vs. the total annual cost of power generation and simulation length

Prediction frame size	**Total Cost [M$]**	**Simulation Duration**	**Average Frame Processing Time**
6	90.68	3h 58[m]	0.28 [sec]
9	90.81	10h 23[m]	0.48 [sec]
12	90.73	15h 26[m]	0.54 [sec]
15	90.66	21h 41[m]	0.59 [sec]
18	90.71	70h 23[m]	1.63 [sec]
24	89.71	94h 56[m]	1.65 [sec]
36	89.75	434h 35[m]	5.03 [sec]

5.5 Simulation including the Voltage Drop Limit effect

To examine the effect of voltage drop limits on the capacity of power transmission lines, two configurations with acceptable voltage drop levels were experimented with and compared to the configuration without the voltage drop constraint. One configuration only allows for 5% voltage drops while the other up to 10%. The considered PFW lengths were 12 and 24 hours and the maximum demand of St. John's was set to 710 MW in all seven cases of the prediction frame window.

The simulation results for the first two weeks of December 2006 using 24 hour PFW are shown in Figures 5.10 and 5.11. They show that using the more limited 5% rule, the hydroelectric power generation limit remains between 309.34 MW and 335.40 MW. It is significantly less than the generation capacity of Bay d'Espoir and the transmission capacity calculated using DTR. In this case, it is not possible to transmit the majority of the demanded energy from hydroelectric generating station;

therefore, the Holyrood thermal station is used constantly. On the other hand, in the 10% case, Bay d'Espoir is producing nearly all the energy and only a small portion of demand is supplied by Holyrood.

The results of using 5% and 10% limits for voltage drop constraint with the case without voltage drop restriction are presented in Tables 5.9 and 5.10. It is shown that the use of the 5% limit results in utilizing the thermal power plant 28.40% of the year, while for the 10% case the thermal share is only 1.44%. In the 5% case, compared to the case without the voltage drop constraint, the generation share of the thermal plant has a significant cost increase of $119.69M. Using the 10% constraint, frequent start-ups of the thermal power plant and the associated costs are avoided during spring and summer, and minimized in fall. However, the number of start-ups in winter increases from 1 to 55. The increased number of start-ups might be seen as an increase in cost. However, this increase indicates that the thermal power plant is used less frequently in the 10% case and the total cost is decreased. Additionally, comparing the 10% case with the one without voltage drop limitation shows that the overall costs of the system are nearly equal in these two configurations.

In the simulated year of 2006, as the restricted power generation of Bay d'Espoir is not sufficient to cover the demand during summer, there is a 6.85% increase in total cost in the 10% voltage drop limited case. This increase of the total cost in the 10% case is the result of using the thermal plant in winter when the constrained generation of the Bay d'Espoir plant is not enough to supply the required demand. The seasonal numerical results in all simulations suggest that energy demand is lowest when the average temperature is relatively high in spring and summer and reaches its maximum when the temperature is relatively low in winter.

Table 5.9: Simulation results using voltage drop constraints of 5% and 10% limits.

	Annual	**Spring**	**Summer**	**Fall**	**Winter**
			Without Voltage Drop Limit		
Cost [M$]	76.48	19.12	19.54	18.91	19.11
Start-up Cost [K$]	97.23	0	0	0.0	97.23
Generated Power [GW]	3459.97	813.31	573.25	896.17	1177.24
Losses [GW]	178.36	39.21	20.79	48.46	69.92
Losses/Generation %	5.16%	4.82%	3.63%	5.41%	5.94%
Maximum Demand [MW]	710.00	563.05	348.47	611.01	710.00
Hydro Gen. Share	99.84%	100.0%	100.0%	100.0%	99.53%
Thermal Gen. Share	0.16%	0%	0%	0.0%	0.47%
# of Start-ups	11	0	0	0	11
			10% Voltage Drop Limit, 24 hour PFW		
Cost [M$]	82.85	19.12	19.54	19.68	24.51
Start-up Cost [K$]	580.86	0	0	89.90	490.96
Generated Power [GW]	3419.79	804.74	570.34	883.30	1161.41
Losses [GW]	138.18	30.64	17.88	35.59	54.08
Losses/Generation %	4.04%	3.81%	3.13%	4.03%	4.66%
Maximum Demand [MW]	710.00	563.05	348.47	611.01	710.00
Hydro Gen. Share	98.56%	100%	100%	99.41%	96.22%
Thermal Gen. Share	1.44%	0%	0%	0.59%	3.78%
# of Start-ups	65	0	0	10	55
			5% Voltage Drop Limit, 24 hour PFW		
Cost [M$]	200.96	45.38	26.14	52.37	77.06
Start-up Cost [K$]	1313.77	366.76	584.09	353.92	9.00
Generated Power [GW]	3347.13	789.82	564.49	864.63	1128.19
Losses [GW]	65.54	15.71	12.02	16.92	20.88
Losses/Generation %	1.96%	1.99%	2.13%	1.96%	1.85%
Maximum Demand [MW]	710.00	563.05	348.47	611.01	710.00
Hydro Gen. Share	71.60%	74.86%	91.82%	70.62%	59.95%
Thermal Gen. Share	28.40%	25.14%	8.18%	29.38%	40.05%
# of Start-ups	148	41	66	40	1

Table 5.10: Simulation results of applying voltage drop constraint to the model using 5 and 10 percent limits.

	Annual	**Spring**	**Summer**	**Fall**	**Winter**
			10% Voltage Drop Limit, 12 hour PFW		
Cost [M$]	82.99	19.12	19.54	19.71	24.63
Start-up Cost [K$]	607.10	0	0	98.90	508.19
Generated Power [GW]	3417.21	804.14	568.64	883.08	1161.34
Losses [GW]	135.60	30.04	16.18	35.37	54.01
Losses/Generation %	3.97%	3.74%	2.84%	4.01%	4.65%
Maximum Demand [MW]	710.00	563.05	348.47	611.01	710.00
Hydro Gen. Share	98.54%	100%	100%	99.40%	96.16%
Thermal Gen. Share	1.46%	0%	0%	0.60%	3.84%
# of Start-ups	68	0	0	11	57
			5% Voltage Drop Limit, 12 hour PFW		
Cost [M$]	201.00	45.42	26.14	52.37	77.06
Start-up Cost [K$]	1327.96	380.95	584.09	353.92	9.00
Generated Power [GW]	3347.19	789.84	564.49	864.66	1128.20
Losses [GW]	65.60	15.73	12.03	16.96	20.88
Losses/Generation %	1.96%	1.99%	2.13%	1.96%	1.85%
Maximum Demand [MW]	710.00	563.05	348.47	611.01	710.00
Hydro Gen. Share	71.61%	74.86%	91.82%	70.65%	59.95%
Thermal Gen. Share	28.39%	25.14%	8.18%	29.35%	40.05%
# of Start-ups	150	43	66	40	1

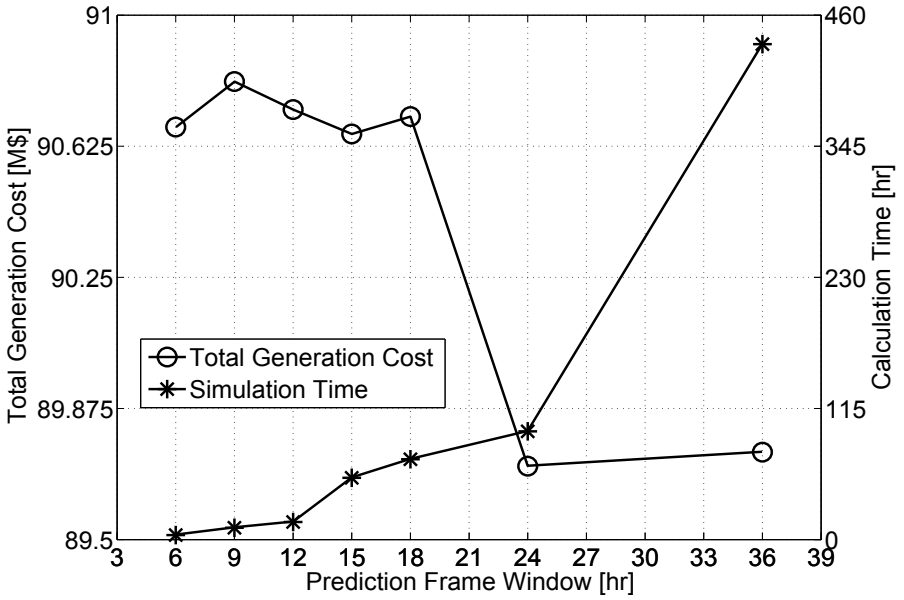

Figure 5.9: Total Generation Cost (Left Y-Axis) and Simulation Duration (Right Y-Axis) vs. Prediction Frame Length (X-Axis)

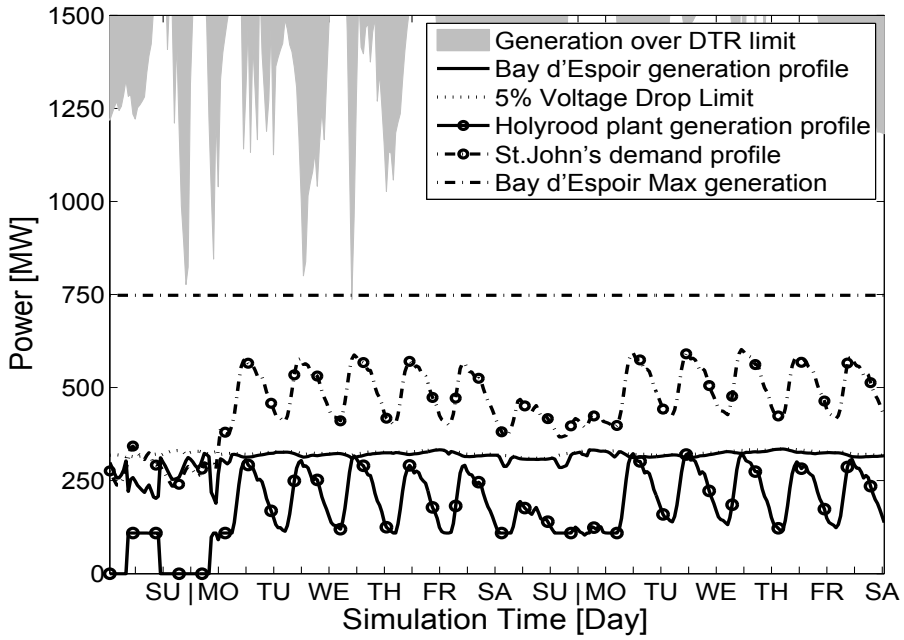

Figure 5.10: Generator scheduling results applying 5% voltage drop constraint on a 2 week sample of load profile

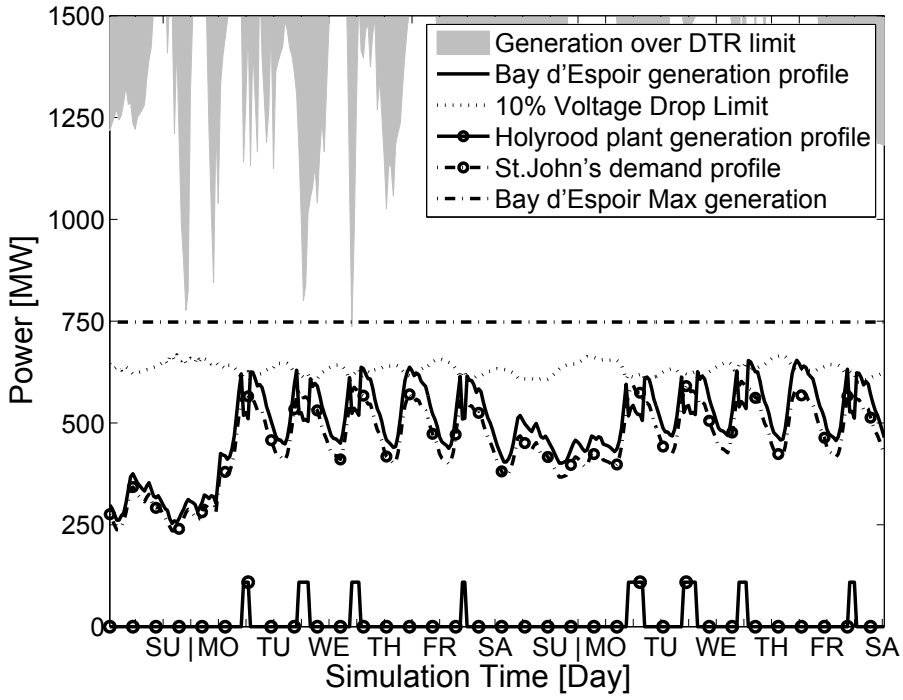

Figure 5.11: Generator scheduling results applying 10% voltage drop constraint on a 2 week sample of load profile

Chapter 6

Conclusions

This work shows the significance of dynamic modeling of the impact of weather on existing power transmission systems. The proposed ED approach for minimizing power generation costs includes considering weather conditions on power transmission systems, voltage drop considerations, and multi-snapshot simulation. Various simulation scenarios for evaluating the performance of the algorithm on a power system were defined and experimented. The optimal performance of the DTR method and the proposed MIP model for economic operation of the entire system is clearly indicated in the results of the simulations.

Moreover, the results suggest that, in general, systems using DTR can transfer more power and allow for more dynamic ampacity compared to the STR or classic baseload methods. The additional ampacity provides an opportunity to transfer power from less expensive sources and reduce the overall cost of the system. In addition, optimized ED using DTR/STR methods outperforms the traditional baseload generation. By using the transmission lines' dynamic ratings and utilizing the less expensive power plant as the primary generating unit, the proposed method enables

the optimization model to exploit the hydro plant's maximum generation capacity and provide the remaining shares of the power from the other generation sources in the network. A typical example of such a configuration is the presented case study, a thermal plant positioned close to a load centre, and a hydroelectric plant located at a rather longer distance.

Seasonal simulation outputs are also presented in all configurations together with the annual results. The characteristics of the model for different seasons and under varying meteorological conditions are illustrated by the results of these simulations. These results demonstrate that start-up costs of the thermal generator, among the other various costs associated with the power plants, is an influential factor which can increase the cost of the entire system. Therefore, lower costs and improved economic performance of the model can be achieved by preventing unnecessary start-ups of the fossil-fuel burning thermal plant.

Experiments with different prediction frame windows suggest that the cost of the entire system decreases slightly by increasing window length and the 24 hour long PFW provides the optimal frame size. Therefore, it is possible to suggest that the model's accuracy would improve by increasing the window length. This can be achieved by improved utilization of demand and meteorological data. Nevertheless, by increasing the prediction frame window, the exponential increase of the simulation time is unavoidable.

Voltage drop limitation, based on two levels of 5% or 10%, is implemented as another rule in the model and its results are presented in the last part of simulations. Comparison of different configuration results shows that the strict 5% voltage drop limit leads to a considerable increase of the system's overall costs. However, this constraint can offer a more stable power transmission by increasing the costs of the

entire system.

6.1 Contributions

The mixed integer programing model, developed in this thesis, provides an optimization tool for economic dispatch in power generation and transmission networks. Contributions of this thesis and important results can be summarized as follows

- The use of DTR leads to improved calculation of transmission line rating. The additional realized capacity of transmission lines allows for more efficient dispatch of energy within the network.
- The multi-snapshot feature, using forecasts of meteorological conditions and load, is capable of dealing with the start-up delay of the thermal power plants and reducing the overall system costs.
- Non-linear convex features of generators and transmission lines can be included in the MIP linear model as linear piecewise equivalents using the proposed approximation method.
- Segment by segment analysis of the transmission line illustrates a significant spatial variability of ampacity and resistance of the line.
- Analysis of the influence of voltage drop on transfer of power over long distances confirm that voltage drop is a significant constraint that may overshadow the effects of thermal constraints.
- The operation of the proposed model has been examined under a number of conditions such as different seasons, varying demand, the use of spinning

reserve, and enforcing voltage drop constraint.

6.2 Future Work

There are several non-linear characteristics of a power plant which the present model lacks because of linearity restrictions. The Valve Point effect of the thermal power plants is an example of such a characteristic. The current model assumes that the relationship between thermal plant generation and the cost associated with it is linear. However, the cost function of a thermal power plant, including the valve point effect, is a superposition of sinusoidal and quadratic functions [55]. This issue can be solved by using a non-linear model of the power plant, which itself will result in having a non-linear power generation and transmission network model. In order to solve this issue, a non-linear modeling technique must be employed.

Hydro power plant reservoir limitation is another issue that is not implemented in the current study. There are several restrictions that can be taken into account such as total reservoir capacity, the amount of flow released, minimum reservoir capacity, minimum generation limit, and the variable cost of generation which is a function of the amount of water that is released by dam [56]. The future model would include these restrictions.

Bibliography

[1] Huneault, M. and Galiana, F.D. and Gross, G., "A Review of Restructuring in the Electricity Business," in 13th Power Syst. Comput. Conf., Jul. 1999, pp. 19–34.

[2] Lai, L.L., Power System Restructuring and Deregulation: Trading, Performance and Information Technology, Wiley, 2001.

[3] Koval, D., "Transmission lines ampacity notes," 1996.

[4] Deb, A.K., Powerline Ampacity System, Theory, Modeling and Applications, CRC Press, 2000.

[5] Frysinger, J.R. et al., "IEEE Standard for Calculating the Current-Temperature of Bare Overhead Conductors," Tech. Rep., IEEE, 2006.

[6] House, H.E. and Tuttle, P.D., "Current-carrying capacity of ACSR," Power Apparatus and Systems, Part III, Transactions of the American Institute of Electrical Engineers, vol. 77, no. Issue:3, pp. 1169–1173, Apr. 1958.

[7] Pytlak, P. and Musilek, P. and Lozowski, E., "Precipitation-based conductor cooling model for dynamic thermal rating systems," in Electrical Power Energy Conference (EPEC), 2009 IEEE, Oct. 2009, pp. 1 –7.

[8] Zhang, P. and Shao, M. and Leoni, A.R. and Ramsay, D.H. and Graham, M., "Determination of static thermal conductor rating using statistical analysis method," in Electric Utility Deregulation and Restructuring and Power Technologies, 2008. DRPT 2008. Third International Conference on, Apr 2008, pp. 1237 –1243.

[9] Roberts, D. and Taylor, P. and Michiorri, A., "Dynamic thermal rating for increasing network capacity and delaying network reinforcements," in Smart Grids for Distribution, 2008. IET-CIRED. CIRED Seminar, Jun 2008, pp. 1 –4.

[10] Adapa, R. and Douglass, D.A., "Dynamic thermal ratings: Monitors and calculation methods," in IEEE Power Engineering Society Inaugural Conference and Exposition in Africa, Jul. 2005.

[11] Talaq, J.H. and El-Hawary, F. and El-Hawary, M.E., "A Summary of Environmental/Economic Dispatch Algorithms," Power Systems, IEEE Transactions on, vol. 9, no. 3, pp. 1508 –1516, Aug. 1994.

[12] Mahor, A. and Prasad, V. and Rangnekar, S., "Economic dispatch using particle swarm optimization: A review," Renewable and Sustainable Energy Reviews, vol. 13, no. 8, pp. 2134–2141, 2009.

[13] Selanduray, H. and Boosroh, M.H., "Power plant optimization in a regulated environment electricity supply industry: A least cost generation approach," in Power and Energy Conference, 2008. PECon 2008. IEEE 2nd International. Dec. 2008, IEEE.

[14] Chowdhury, B.H. and Rahman, S., "A review of recent advances in economic dispatch," Power Systems, IEEE Transactions on, vol. 5, no. 4, pp. 1248 –1259, nov 1990.

[15] Garver, L., "Transmission Network Estimation Using Linear Programming," IEEE Transactions on Power Apparatus and Systems, vol. PAS-89, Issue:7, no. 7, pp. 1688–1697, Sep./Oct. 1970.

[16] Moon, Y.H. and Park, J.D. and Lee, Y.H. and Lee, T.S., "A new economic dispatch algorithm for thermal unit generation scheduling in power system," Power Engineering Society Winter Meeting, vol. 2, pp. 1034–1039, Jan. 2000.

[17] Chung, T.S. and Shaoyun, G.E., "A recursive LP-based approach for optimal capacitor allocation with cost-benefit consideration," Electric Power Systems Research, vol. 39, no. 2, pp. 129 – 136, 1996.

[18] Karmarkar, N., "A new polynomial-time algorithm for linear programming," in Proceedings of the sixteenth annual ACM symposium on Theory of computing, New York, NY, USA, 1984, STOC '84, pp. 302–311, ACM.

[19] Momoh, J.A., "A generalized quadratic-based model for optimal power flow," in Systems, Man and Cybernetics, 1989. Conference Proceedings., IEEE International Conference on, Nov 1989, pp. 261 –271 vol.1.

[20] Zhu, J. and Momoh, J.A., "Multi-area power systems economic dispatch using nonlinear convex network flow programming," Electric Power Systems Research, vol. 59, no. 1, pp. 13 – 20, 2001.

[21] Chowdhury, B.H., "Toward the concept of integrated security: optimal dispatch under static and dynamic security constraints," Electric Power Systems Research, vol. 25, no. 3, pp. 213 – 225, 1992.

[22] Chen, P.H. and Chang, H.C., "Large-Scale Economic Dispatch by Genetic Algorithm," Power Systems, IEEE Transactions on, vol. 10, no. 4, pp. 1919 –1926, Nov 1995.

[23] Somasundaram P., Kuppusamy K., and R.P. Devi, "Evolutionary Programming based Security Constrained Optimal Power Flow," Electric Power Systems Research, vol. 72, no. 2, pp. 137 – 145, 2004.

[24] Yoshida, H. and Kawata, K. and Fukuyama, Y. and Takayama, S. and Nakanishi, Y., "A particle swarm optimization for reactive power and voltage control considering voltage security assessment," Power Systems, IEEE Transactions on, vol. 15, no. 4, pp. 1232 –1239, Nov 2000.

[25] Yu, I.K. and Song, Y.H., "A novel short-term generation scheduling technique of thermal units using ant colony search algorithms," International Journal of Electrical Power and Energy Systems, vol. 23, no. 6, pp. 471 – 479, 2001.

[26] Espinoza, M. and Suykens, J.A.K. and Belmans, R. and De Moor, B., "Electric Load Forecasting: Using kernel-based modeling for nonlinear system identification," IEEE Control Systems Magazine, pp. 43–57, Oct. 2007.

[27] Gonen, T., Electric Power Transmission System Engineering: Analysis and Design, John Wiley and Sons, 1988.

[28] Douglass, D.A., "Weather-Dependent versus Static Thermal Ratings," IEEE Transaction on Power Delivery, vol. 3, no. 2, pp. 742–753, Apr. 1998.

[29] Douglass, D.A. and Edris, A.A., "Real-Time Monitoring and Dynamic Thermal Rating of Power Transmission Circuits," IEEE Transaction on Power Delivery, vol. 11, no. 3, pp. 1407–1418, Jul. 1996.

[30] Banakar, H. and Alguacil, N. and Galiana, F.D., "Electrothermal Coordination Part I, Theory and Implementation Schemes," IEEE Transactions on Power Systems, vol. 20, Issue 2, no. 2, pp. 798–805, May 2005.

[31] Davis, M.W., "A new thermal rating approach: The real time thermal rating system for strategic overhead conductor transmission lines – Part I: General description and justification of the real time thermal rating system," IEEE Transactions on Power Apparatus and Systems, vol. 96, no. 3, pp. 803–809, 1977.

[32] Ciniglio, O.A. and Deb, A.K., "Optimizing Transmission Path Utilization in Idaho Power," IEEE Transactions on Power Delivery, vol. 19, no. 2, pp. 830–834, Apr. 2004.

[33] Alguacil, N. and Banakar, M.H. and Galiana, F.D., "Electrothermal Coordination Part II: Case Studies," IEEE Transactions on Power Systems, vol. 20, no. 4, pp. 1738–1745, Nov. 2005.

[34] Saied, M.M., "Assessing the dynamic rating of overhead transmission lines," European Transactions on Electrical Power, vol. 17, issue 5, pp. 526–536, Jan. 2007.

[35] Wright Sh.H. and Hall C.F. and Shankle D.F. and Tremaine R.L., Electrical Transmission and Distribution Reference Book, Chapter 3, Electric Systems Technology Institute, ABB Power T&D Company Inc.©, 1997.

[36] Phoenix Wire©, "Bare Overhead Conductors, Aluminum Conductor Steel Reinforced ACSR," http://www.phoenixwc.com.

[37] Sural©, "PRODUCT CATALOG ACSR (Aluminum Conductor, Steel Reinforced)," http://www.sural.com.

[38] Kiessling, F. and Nefzger, P. and Nolasco, J.F. and Kaintzyk, U., Overhead power lines, planning design construction, Springer-Verlag, 2003.

[39] Billinton, R. and Kumar, S. and Chowdhury, N. and Chu, K. and Debnath, K. and Goel, L. and Khan, E. and Kos, P. and Nourbakhsh, G. and Oteng-Adjei, J., "A reliability test system for educational purposes-basic data," Power Systems, IEEE Transactions on, vol. 4, no. 3, pp. 1238 –1244, Aug. 1989.

[40] Park, Y.M. and Park, J.B. and Won, J.R., "A hybrid genetic algorithm/dynamic programming approach to optimal long-term generation expansion planning," International Journal of Electrical Power and Energy Systems, vol. 20, no. 4, pp. 295–303, 1998.

[41] Park, Y.M. and Won, J.R. and Park, J.B. and Kim, D.G., "Generation expansion planning based on an advanced evolutionary programming," IEEE Transactions on Power Systems, vol. 14, no. 1, pp. 299 –305, Feb. 1999.

[42] Wang, C. and Shahidehpour, S.M., "Effects of ramp-rate limits on unit commitment and economic dispatch," IEEE Transactions on Power Systems, vol. 8, no. 3, pp. 1341 –1350, Aug. 1993.

[43] Ouyang, Z. and Shahidehpour, S.M., "Heuristic multi-area unit commitment with economic dispatch," IEEE Proceedings C, Generation, Transmission and Distribution, vol. 138, no. 3, pp. 242 –252, May 1991.

[44] Pindoriya, N.M. and Singh, S.N. and Stergaard, J., "Day-Ahead Self-Scheduling of Thermal Generator in Competitive Electricity Market Using Hybrid PSO," in Intelligent System Applications to Power Systems, 2009. ISAP '09. 15th International Conference on, 8-12 2009, pp. 1 –6.

[45] Lee, K. Y. and El-Sharkawi, M.A., Ed., Modern Heuristic Optimization Techniques, Theory and Applications to Power Systems, CRC Press, 2008.

[46] Rebours, Y. and Kirschen, D., "What is spinning reserve?," Tech. Rep., The University of Manchester, Sep. 2005.

[47] Morgan, V.T., "Effects of alternating and direct current, power frequency, temperature, and tension on the electrical parameters of ACSR conductors," Power Delivery, IEEE Transactions on, vol. 18, no. 3, pp. 859 – 866, Jul. 2003.

[48] Earley W.M. and Sargent J.S. and Sheehan J.V. and Buss W.E., National Electrical Code Handbook, Cengage Learning, Eleventh edition, 2008.

[49] Adapa, R., Increased Power Flow Guidebook, Increasing Power Flow in Transmission and Substation Circuits, EPRI, 2005.

[50] Fourer R., AMPL, A Modeling Language for Mathematical Programming, Thomson Books/Cole, Second edition, 2003.

[51] Mesinger, F. et al., "North American Regional Reanalysis," , no. 3, 2006, pp. 343-360.

[52] Newfoundland and Labrador Hydro, "Business and financial report," Tech. Rep., 2007.

[53] "IEEE Standard for Calculating the Current-Temperature of Bare Overhead Conductors," Nov. 2006.

[54] P.M. Callahan and D.A. Douglass, "An experimental evaluation of a thermal line uprating by conductor temperature and weather monitoring," Power Delivery, IEEE Transactions on, vol. 3, no. 4, pp. 1960 –1967, Oct. 1988.

[55] Park, J.B. and Lee, K.S. and Shin, J.R. and Lee, K.Y., "A particle swarm optimization for economic dispatch with nonsmooth cost functions," Power Systems, IEEE Transactions on, vol. 20, no. 1, pp. 34 – 42, feb. 2005.

[56] Forsund, F.R., Hydropower Economics, Springer, 2007.